CONVEX RELAXATION OF DISCRETE VECTOR-VALUED OPTIMIZATION PROBLEMS

Christian Clason[*] Carla Tameling[†] Benedikt Wirth[‡]

Abstract We consider a class of infinite-dimensional optimization problems in which a distributed vector-valued variable should pointwise almost everywhere take values from a given finite set $\mathcal{M} \subset \mathbb{R}^m$. Such hybrid discrete–continuous problems occur in, e.g., topology optimization or medical imaging and are challenging due to their lack of weak lower semicontinuity. To circumvent this difficulty, we introduce as a regularization term a convex integral functional with an integrand that has a polyhedral epigraph with vertices corresponding to the values of $\mathcal{M}$; similar to the L^1 norm in sparse regularization, this "vector multibang penalty" promotes solutions with the desired structure while allowing the use of tools from convex optimization for the analysis as well as the numerical solution of the resulting problem.

We show well-posedness of the regularized problem and analyze stability properties of its solution in a general setting. We then illustrate the approach for three specific model optimization problems of broader interest: optimal control of the Bloch equation, optimal control of an elastic deformation, and a multimaterial branched transport problem. In the first two cases, we derive explicit characterizations of the penalty and its generalized derivatives for a concrete class of sets $\mathcal{M}$. For the third case, we discuss the algorithmic computation of these derivatives for general sets. These derivatives are then used in a superlinearly convergent semismooth Newton method applied to a sequence of regularized optimization problems.

We illustrate the behavior of this approach for the three model problems with numerical examples.

1 INTRODUCTION

Many optimization problems involve minimizing the distance of a quantity $S(u)$ to some given z, where u is the optimization variable and $S(u)$ denotes the output of some model depending on u. This may arise either from an optimal control problem, in which we try to choose the control u such that the state $y = S(u)$ – commonly the solution to a differential equation – comes close to a desired state z, or from an inverse problem, in which a measurement z has been obtained via a forward operator S from a physical configuration u, which we try to recover. Typically u is from an infinite-dimensional function space. To make the problem well-posed, a regularization usually has to be incorporated, which encodes some a priori knowledge or requirement of u. Such a priori knowledge could for instance be the fact

CC was supported by the German Science Fund (DFG) under grant CL 487/1-1. CT gratefully acknowledges support by the DFG Research Training Group 2088 Project A1. BW is supported by the German Science Fund (DFG) under the priority program SPP 1962, grant WI 4654/1-1, and under Germany's Excellence Strategy EXC 2044 – 390685587, Mathematics Münster: Dynamics–Geometry–Structure.

[*]Faculty of Mathematics, Universität Duisburg-Essen, 45117 Essen, Germany; *current address:* Institute of Mathematics and Scientific Computing, University of Graz, Heinrichstrasse 36, 8010 Graz, Austria (c.clason@uni-graz.at, orcid: 0000-0002-9948-8426)

[†]Institute for Mathematical Stochastics, Universität Göttingen, Goldschmidtstr. 7, 37077 Göttingen, Germany (carla.tameling@mathematik.uni-goettingen.de)

[‡]Applied Mathematics, Universität Münster, Einsteinstr. 62, 48149 Münster, Germany (benedikt.wirth@uni-muenster.de, orcid: 0000-0003-0393-1938)

that u pointwise almost everywhere takes values only from a prescribed finite set $\mathcal{M} \subset \mathbb{R}^m$ for some $m \in \mathbb{N}$, which is the situation we will focus on. Examples include topology optimization, where the spatial material composition of a (mechanical) structure is optimized and in which $\mathcal{M}$ comprises the material parameters of the available material components, or inverse problems in which the spatial distribution of a few known materials (or, in medical imaging, tissues with known properties) has to be identified. Our goal is to achieve this using a *convex* regularization so that we can apply elegant and powerful tools from convex optimization for its analysis and numerical solution.

Specifically, in this work we consider the optimization problem

$$\min_{u\in U} \frac{1}{2}\|S(u) - z\|_Y^2 + \int_\Omega g(u(x))\,\mathrm{d}x, \tag{1.1}$$

where $\Omega \subset \mathbb{R}^n$ is an open bounded domain, $U = L^2(\Omega;\mathbb{R}^m)$ for some $m \geq 2$, Y is a Hilbert space, $z \in Y$, $S\colon U \to Y$ is a compact and Fréchet differentiable (possibly nonlinear) operator, and the pointwise *vector multibang penalty* $g\colon \mathbb{R}^m \to \mathbb{R} \cup \{\infty\}$ has a convex polyhedral epigraph and superlinear growth at infinity. This extends the class of scalar problems considered in [17, 18] to the vector-valued case, and our main interest in this article is the behavior and influence of this vector multibang penalty on the solution, which we will study by way of examples for three different operators S (the solution operators of the Bloch equation and of linearized elasticity as well as the graph divergence for a branched transport model) and specific costs g (whose graph is given by a polyhedral cone, a square frustum, and a more general polyhedron in $\mathbb{R}^{m+1}$, respectively). The basic underlying intuition for our specific choice of the term $\int_\Omega g(u(x))\,\mathrm{d}x$ is that this regularization in combination with a quadratic discrepancy term increasingly promotes values of u on lower-dimensional facets and, in particular, at the vertices of the graph of g, since the linear growth away from a vertex will lead to a comparatively greater increase in the penalty than the corresponding decrease in the discrepancy term. The same mechanism is responsible for the sparsity-promoting property (i.e., the preference for $u = 0$) of L^1 regularization; it is also related to the fact that in linear optimization, minima are always found at a vertex of the polyhedral feasible set. The central idea of our approach is to design the penalty g such that these vertices correspond precisely to the elements of the set $\mathcal{M}$, which we will make more precise in the following.

Motivation Formulating the original optimal control or inverse problem directly over the set of discrete-valued desired solutions leads to the minimization of the energy

$$\mathcal{E}^{\mathcal{M}}(u) = \frac{1}{2}\|S(u) - z\|_Y^2 + \int_\Omega \delta_{\mathcal{M}}(u(x))\,\mathrm{d}x \qquad \text{with } \delta_{\mathcal{M}}(v) = \begin{cases} 0 & \text{if } v \in \mathcal{M}, \\ \infty & \text{otherwise.} \end{cases}$$

Unfortunately, $\mathcal{E}^{\mathcal{M}}$ is not weakly lower semicontinuous [10, Cor. 2.14] so that the problem is ill-posed (unless the inverse operator S^{-1} is compact into $L^1(\Omega;\mathbb{R}^m)$), in which case the energy is strongly coercive in $L^1(\Omega;\mathbb{R}^m)$ and one would only require strong lower semicontinuity): generically there are no minimizers, and controls u with small energy $\mathcal{E}^{\mathcal{M}}(u)$ will rapidly oscillate between different values in $\mathcal{M}$. There are (at least) two possible ways out:

(i) The first approach adds a penalty of variations of u, for instance the total variation seminorm $\|u\|_{TV} = \int_\Omega \mathrm{d}|\nabla u|$ or a Mumford–Shah-type regularization functional, which has the effect of preventing oscillations and penalizing the interfaces between regions of different values of u. A disadvantage of this approach is that it quite explicitly regularizes the geometry of the material distribution, which is the sought quantity. For instance, such a regularization will lead to rounded-off interfaces that cannot have corners.

(ii) The second approach considers instead the relaxation (i.e., the lower semi-continuous envelope) of $\mathcal{E}^{\mathcal{M}}$, thereby admitting also mixed control values $u(x) \notin \mathcal{M}$ that represent mixtures of values in $\mathcal{M}$. This is an obvious disadvantage; however, it might be alleviated by adding a convex (to ensure weak lower semicontinuity) cost $\int_\Omega c(u(x))\,\mathrm{d}x$ that may, for instance, encode a known preference for a certain material. If this is done before relaxation, then mixed control values will no longer have equal costs to pure control values so that the relaxation may again lead to pure control values $u(x) \in \mathcal{M}$. This has for instance been observed in [17].

The additional cost regularization of the latter approach acts on the material amounts rather than the geometry of their distribution and therefore is worthwhile studying as an alternative to the standard regularization via penalization of interfaces. Specifically, the relaxation of $\int_\Omega \delta_{\mathcal{M}}(u(x))\,\mathrm{d}x+\alpha\int_\Omega c(u(x))\,\mathrm{d}x$ for some $\alpha > 0$ and $c : \mathbb{R}^m \to \mathbb{R}$ nonnegative, strictly convex, and lower semicontinuous, is given by $\int_\Omega g(u(x))\,\mathrm{d}x$ with

$$g = g_\infty^{**} \qquad \text{for } g_\infty := \alpha c + \delta_{\mathcal{M}}, \tag{1.2}$$

where the double asterisk denotes the biconjugate or convex envelope. The functions g are precisely those with a convex polyhedral epigraph (since this epigraph is the convex hull of the finitely many points $\{(v, \alpha c(v))) : v \in \mathcal{M}\}$, and any function g with convex polyhedral epigraph can be obtained via $c = g/\alpha$ and an appropriate choice of $\mathcal{M}$), which motivates our problem formulation (1.1). While our theoretical results will hold for any such choice of c, the explicit computation of g and the numerical solution will be carried out as in [15, 17, 18] mostly for the two specific choices

$$c(v) = \frac{1}{2}|v|_2^2 \qquad \text{and} \qquad c(v) = |v|_2.$$

In the case of a scalar function u (i.e., for $m = 1$) and the first choice of c, this optimization problem reduces to the one considered in [17]; the difference in the vector-valued case is that now several (or even all) values in $\mathcal{M}$ can be assigned the same control cost, therefore allowing for multiple equally preferred discrete values. Providing explicit and numerically implementable characterizations of the required generalized derivatives is one of the main contributions of this work. Furthermore, we provide an extended analysis of the stability and multibang properties of the optimal controls in the general case.

Model problems To illustrate the broad applicability of the proposed approach, we consider as specific examples three different forward operators S and admissible sets $\mathcal{M}$ (the analysis in Sections 2 to 4 will be independent of these models, though, beyond some general assumptions).

The first example follows [25], where the authors try to drive a collection of spin systems using external electromagnetic fields to a desired spin state in the context of NMR spectroscopy or tomography. The hardware here only allows a discrete set of control values (the radiofrequency pulse phases and amplitudes). The underlying model is given by the Bloch equation in a rotating reference frame without relaxation (see [27] for an introduction), which relates the magnetization vector $\mathbf{M} : [0,T] \to \mathbb{R}^3$ and the applied magnetic field $\mathbf{B} : [0,T] \to \mathbb{R}^3$ via the bilinear differential equation

$$\frac{\mathrm{d}}{\mathrm{d}t}\mathbf{M}(t) = \mathbf{M}(t) \times \mathbf{B}(t), \qquad \mathbf{M}(0) = \mathbf{M}_0.$$

The goal is to shift the magnetization vector from the initial state $\mathbf{M}_0$ (e.g., aligned to a strong external field) to a desired state $\mathbf{M}_d$ (e.g., orthogonal to the external field) at time T. The control $u \in L^2((0,T);\mathbb{R}^2)$ enters the equation as $\mathbf{B}(t) = (u_1(t), u_2(t), \omega)$, where ω is a fixed resonance frequency (which coincides with the rotation frequency of the domain), and thus the (nonlinear) operator S maps the control u onto the magnetization vector $\mathbf{M}(T)$ at time T. For details, see Section 5.1.

The second example deals with linearized elasticity as the most basic model of coupled PDEs as state equations, i.e., we consider S to be the solution operator of the elliptic problem

$$\begin{cases} -2\mu \operatorname{div} \epsilon(y) - \lambda \operatorname{grad} \operatorname{div} y = u \text{ in } \Omega, \\ y = 0 \text{ on } \Gamma, \\ (2\mu\epsilon(y) + \lambda \operatorname{div} y)n = 0 \text{ on } \partial\Omega \setminus \Gamma, \end{cases}$$

with distributed control u; see Section 5.2 for details.

The third example illustrates applications to more general variational problems and concerns multimaterial branched transport as introduced in [38]. Here, different materials have to be transported through a street or pipe network, where for each material i the amount m_i has to be routed from its source x_i to its sink y_i. The flux along a street or pipe is described by the vector-valued function u defined on the network, where u_i describes the flux of material i with its sign indicating the flow direction. To avoid an uneconomic splitting of each material, $\mathcal{M}$ should only contain vectors corresponding to combinations of (positive or negative, depending on direction) fluxes m_i of different materials. The cost c may in addition favor certain combinations over others (e.g., if joint transport of two materials is particularly economic). The operator S here describes the divergence of the flux, and the deviation of Su from $z = \sum_i m_i e_i(\delta_{x_i} - \delta_{y_i})$ (with e_i the ith standard unit vector and δ_x the Dirac measure at x) is penalized to avoid material loss.

Regarding the admissible set $\mathcal{M}$, we consider for the case of the Bloch equation – again following [25] – radially distributed control values together with the origin, i.e.,

$$\mathcal{M} = \left\{ \begin{pmatrix} 0 \\ 0 \end{pmatrix}, \begin{pmatrix} \omega_0 \cos\theta_1 \\ \omega_0 \sin\theta_1 \end{pmatrix}, \dots, \begin{pmatrix} \omega_0 \cos\theta_M \\ \omega_0 \sin\theta_M \end{pmatrix} \right\}$$

for a fixed amplitude $\omega_0 > 0$ and $M > 2$ equidistributed phases

$$0 \le \theta_1 < \cdots < \theta_M < 2\pi.$$

In this example, all admissible control values apart from 0 have the same magnitude; it also provides a link to classical sparsity promotion and allows a closed-form treatment of an arbitrary number of such states.

For the case of linearized elasticity, we consider in addition an admissible set containing control values of different magnitudes but not the origin. As an example, we make the concrete choice

$$\mathcal{M} = \left\{ \begin{pmatrix} 1 \\ 1 \end{pmatrix}, \begin{pmatrix} 1 \\ -1 \end{pmatrix}, \begin{pmatrix} -1 \\ 1 \end{pmatrix}, \begin{pmatrix} -1 \\ -1 \end{pmatrix}, \begin{pmatrix} 2 \\ 2 \end{pmatrix}, \begin{pmatrix} 2 \\ -2 \end{pmatrix}, \begin{pmatrix} -2 \\ 2 \end{pmatrix}, \begin{pmatrix} -2 \\ -2 \end{pmatrix} \right\}.$$

For multimaterial branched transport, the admissible control values are

$$\mathcal{M} = \{u \in \mathbb{R}^m : u_i \in \{0, m_i\} \text{ for } i = 1, \dots, m \text{ or } u_i \in \{0, -m_i\} \text{ for } i = 1, \dots, m\},$$

with $m_1, \dots, m_m > 0$ fixed material amounts. Note that $\mathcal{M}$ only contains vectors with either all nonnegative or all nonpositive components; components with opposite sign would represent different materials flowing in opposite directions, for which there is no economic preference.

Beyond illustrating the general procedure, these examples are meant to be useful prototypes that should be directly applicable.

Related work Convex relaxation of problems lacking weak lower semicontinuity has a long history; here we only mention the monograph [26]. In the context of optimal control of partial differential equations, convex relaxation of discrete control constraints was discussed in [17, 18, 16, 19]; the latter two treating controls in the principal coefficient – leading to challenges related to homogenization theory – in combination with total variation regularization required to overcome these challenges. In the context of inverse problems, the use of the scalar multibang penalty as a regularization term was investigated in [13, 24]; multibang regularization was applied to different imaging problems in [33, 52]. Error estimates for the finite element approximation of such problems can be found in [14]. A similar convex relaxation approach was applied to optimal controls with switching structure in [15]. Special cases were treated much earlier for scalar controls. In particular, if $\mathcal{M}$ contains only two points, problem (1.1) coincides with a (regularized) bang-bang control problem; see, e.g., [6, 48, 49]. For $\mathcal{M} = \{0\}$, the relaxation reduces to the well-known L^1 norm used to promote sparse controls; see, e.g., [47, 11, 35].

There is a vast literature concerning pulse design in magnetic resonance imaging and spectroscopy via optimal control of the Bloch equation, e.g., [22, 46, 43, 36, 53, 29, 30, 45]. A mathematical treatment of this problem can be found in, e.g., [8]. Numerical methods for the computation of optimal pulses are based on conjugate gradient methods (see, e.g., [37]), Krotov methods [51], quasi-Newton and Newton methods with approximate second derivatives [3], and Newton methods using exact second derivatives computed via the adjoint approach [1] (which was also the basis of the winning approaches in the 2015 ISMRM RF Pulse Design Challenge [31]). The latter is the basis for the numerical treatment in this work. To the best of our knowledge, there is so far only a very limited number of works dealing with the design of discrete-valued pulses, which is of interest since the hardware often allows only a finite set $\mathcal{M}$ of pulses [23, 42]. In [25], this problem is treated via an extension of the approach from [36] together with a quantization of a continuous control field obtained via standard optimization methods.

The interest in branched transport as a nonconvex version of optimal transport arose during the past two decades, and the textbook [7] can serve as a comprehensive starting point into the theory. The multimaterial version that we consider here was introduced in [38] as a convexification of the original branched transport problem. So far this approach has numerically only been exploited by computing dual certificates for solutions to particular types of branched transport problems [39].

Organization Section 2 provides the abstract convex analysis framework, including existence of solutions of the optimal control problem, necessary optimality conditions, as well as an appropriate regularization for numerical purposes. Section 3 then derives stability results based on rather general assumptions on the state operator and the multibang penalty. Section 4 gives an explicit characterization of the convex analysis framework for the specific examples of the multibang penalty used in this work, while Section 5 gives more detail about the model state equations and, in particular, verifies for them the previously exploited assumptions. Section 6 discusses the numerical solution using a semismooth Newton method. Finally, Section 7 presents and discusses illustrative numerical examples for the three model problems.

2 CONVEX ANALYSIS FRAMEWORK

To obtain existence of minimizers and numerically feasible optimality conditions, we follow the general framework of [18] (stated there for the scalar case), which we briefly summarize in this section and adapt to the vector-valued case. We refer to, e.g., [4, 44, 12] as well as [21] for a general introduction to nonsmooth analysis and optimization. Recall that $U = L^2(\Omega; \mathbb{R}^m)$ for some bounded open domain

$\Omega \subset \mathbb{R}^n$ and $m \geq 2$, Y is a Hilbert space, and

$$\mathcal{F}: U \to \mathbb{R} \cup \{\infty\}, \quad u \mapsto \tfrac{1}{2}\|S(u) - z\|_Y^2,$$
$$\mathcal{G}: U \to \mathbb{R} \cup \{\infty\}, \quad u \mapsto \textstyle\int_\Omega g(u(x))\,\mathrm{d}x$$

for $g : \mathbb{R}^m \to \mathbb{R} \cup \{\infty\}$ proper, convex, lower semicontinuous with $\operatorname{dom} g = \operatorname{co} \mathcal{M}$ (the convex hull of $\mathcal{M}$) for some finite set $\mathcal{M} \subset \mathbb{R}^m$. Relating properties of the integrand g to the corresponding integral functional $\mathcal{G}$ will be crucial in what follows. For the operator S we will require the following assumptions:

(A1) Weak-to-weak continuity, i.e., $u_i \rightharpoonup u$ in $U \quad \Rightarrow \quad S(u_i) \rightharpoonup S(u)$ in Y.

(A2) Fréchet differentiability.

Throughout, we identify the dual space U^* with U via the Riesz isomorphism.

We now consider the problem

$$\min_{u \in U} \mathcal{E}(u) \quad \text{for } \mathcal{E}(u) := \mathcal{F}(u) + \mathcal{G}(u). \tag{2.1}$$

The following statements are analogous to [18, Props. 2.1 and 2.2] for the vector-valued case.

Proposition 2.1 (existence of minimizers). *Let S satisfy (A1). Then there exists a solution $\bar{u} \in U$ to (2.1).*

Proof. Consider a minimizing sequence $\{u_i\}_{i\in\mathbb{N}}$. Since g is infinite outside of $\operatorname{co} \mathcal{M}$, we know that $\|u_i\|_{L^\infty(\Omega)}$ is uniformly bounded so that we may extract a subsequence, again denoted by $\{u_i\}_{i\in\mathbb{N}}$, weakly converging in U to some $\bar{u} \in U$. Now $\int_\Omega g(u(x))\,\mathrm{d}x$ is sequentially weakly lower semicontinuous by the convexity of g, while property (A1) implies weak convergence $S(u_i) \rightharpoonup S(\bar{u})$ so that

$$\frac{1}{2}\|S(\bar{u}) - z\|_Y^2 + \int_\Omega g(\bar{u}(x))\,\mathrm{d}x \leq \liminf_{i\to\infty} \frac{1}{2}\|S(u_i) - z\|_Y^2 + \int_\Omega g(u_i(x))\,\mathrm{d}x.$$

Hence $\bar{u}$ must be a minimizer. ∎

Proposition 2.2 (optimality conditions). *Let S satisfy (A2) and let $\bar{u} \in U$ be a local minimizer of (2.1). Then there exists a $\bar{p} \in U$ satisfying*

$$\begin{cases} -\bar{p} = \mathcal{F}'(\bar{u}) = S'(\bar{u})^*(S(\bar{u}) - z), \\ \bar{u} \in \partial\mathcal{G}^*(\bar{p}), \end{cases} \tag{2.2}$$

where $S'(u)^* : Y \to U$ denotes the (Hilbert-space) adjoint of the Fréchet derivative of $S : U \to Y$,

$$\mathcal{G}^* : U \to \mathbb{R} \cup \{\infty\}, \qquad p \mapsto \sup_{u\in U} \langle p, u\rangle - \mathcal{G}(u),$$

denotes the Fenchel conjugate of $\mathcal{G}$, and $\partial\mathcal{G}^*$ denotes its convex subdifferential.

Proof. Abbreviate $u_t = \bar{u} + t(u - \bar{u})$ for arbitrary $t > 0$ and $u \in U$. Due to the optimality of $\bar{u}$ we have

$$0 \leq [\mathcal{F}(u_t) + \mathcal{G}(u_t)] - [\mathcal{F}(\bar{u}) + \mathcal{G}(\bar{u})].$$

Dividing by t and rearranging, we arrive at

$$0 \leq \frac{\mathcal{F}(u_t) - \mathcal{F}(\bar{u})}{t} + \frac{\mathcal{G}(u_t) - \mathcal{G}(\bar{u})}{t} \leq \frac{\mathcal{F}(u_t) - \mathcal{F}(\bar{u})}{t} + \frac{(1-t)\mathcal{G}(\bar{u}) + t\mathcal{G}(u) - \mathcal{G}(\bar{u})}{t},$$

where in the second inequality we used the convexity of $\mathcal{G}$. Taking the limit $t \to 0$ and setting $\bar{p} = -\mathcal{F}'(\bar{u})$, we arrive at

$$0 \leq \langle -\bar{p}, u - \bar{u}\rangle + \mathcal{G}(u) - \mathcal{G}(\bar{u}).$$

As this holds for all $u \in U$, we have by definition of the convex subdifferential that $\bar{p} \in \partial\mathcal{G}(\bar{u})$. By the Fenchel–Young Lemma (e.g., [21, Lem. 5.8]), this is equivalent to $\bar{u} \in \partial\mathcal{G}^*(\bar{p})$. ∎

By, e.g., [21, Thms. 4.11 and 5.5], we have the pointwise a.e. expression

$$\partial\mathcal{G}^*(p) = \{u \in U : u(x) \in \partial g^*(p(x)) \text{ for a.e. } x \in \Omega\}, \tag{2.3}$$

where g^* is the Fenchel conjugate of g. It is readily seen that for g chosen as in (1.2), g^* is piecewise affine and thus ∂g^* is single valued in each affine region, the values being precisely the elements of $\mathcal{M}$ (see Section 4). More precisely, for each $u \in \mathcal{M}$ there is an open convex polyhedron $Q(u) \subset \mathbb{R}^m$ such that $\mathbb{R}^m = \bigcup_{u\in\mathcal{M}} \overline{Q(u)}$ and $\partial g^*(q) = \{u\}$ for all $q \in Q(u)$. This property suggests that solutions to (2.2) generically satisfy $u \in \mathcal{M}$ almost everywhere, which will be exploited in Section 3 to derive corresponding stability properties of optimal controls.

Our goal is now to solve (2.2) using a semismooth Newton method in function spaces; see [34, 50] as well as [21, Chap. 14]. This requires constructing a so-called Newton derivative that, used in place of the non-existing Fréchet derivative of $\partial\mathcal{G}^*$ in a Newton step for (2.2), will lead to local superlinear convergence; see, e.g., [21, Thm. 14.1]. This is challenging in general; however, we know by, e.g., [21, Thm. 14.10] that if (and only if) $r > s$, then a superposition operator $H : L^r(\Omega, \mathbb{R}^m) \to L^s(\Omega; \mathbb{R}^m)$ given by $p(x) \mapsto h(p(x))$ for a.e. $x \in \Omega$ and locally Lipschitz continuous $h : \mathbb{R}^m \to \mathbb{R}^m$ is Newton differentiable with Newton derivative $D_N H(p)$ given pointwise a.e. by an arbitrary element of the Clarke subdifferential

$$\partial_C h(q) = \operatorname{co}\left\{\lim_{n\to\infty} \nabla h(q_n)\right\}, \tag{2.4}$$

where $\{q_n\}_{n\in\mathbb{N}} \subset \mathbb{R}^m$ is a sequence of points where h is differentiable with $q_n \to q$; such a sequence always exists in finite dimensions by Rademacher's Theorem; see, e.g., [21, Thm. 13.26].

Since the second relation in (2.2) involves a set-valued mapping, we first need to apply a regularization. Here we replace the subdifferential $\partial\mathcal{G}^*(p)$ by its Yosida approximation

$$(\partial\mathcal{G}^*)_\gamma(p) := \frac{1}{\gamma}\left(p - \operatorname{prox}_{\gamma\mathcal{G}^*}(p)\right) : U \to U \tag{2.5}$$

for some $\gamma > 0$ and the proximal mapping

$$\operatorname{prox}_{\gamma\mathcal{G}^*}(p) := (\mathrm{Id} + \gamma\partial\mathcal{G})^{-1}(p) = \operatorname*{arg\,min}_{\tilde p\in U} \frac{1}{2\gamma}\|\tilde p - p\|_U^2 + \mathcal{G}^*(\tilde p), \tag{2.6}$$

which is single-valued and Lipschitz continuous since $\mathcal{G}^*$ is convex and lower semicontinuous; see, e.g., [21, Thm. 6.11 and Cor. 6.14]. We thus consider instead of (2.2) for $\gamma > 0$ the regularized optimality conditions

$$\begin{cases} -p_\gamma = \mathcal{F}'(u_\gamma), \\ \ \ u_\gamma = (\partial\mathcal{G}^*)_\gamma(p_\gamma). \end{cases} \tag{2.7}$$

By (2.3), we can characterize $\operatorname{prox}_{\gamma\mathcal{G}^*}$ and therefore $H_\gamma := (\partial\mathcal{G}^*)_\gamma$ pointwise a.e. as well; we will derive explicit pointwise expressions for the Yosida approximation and its Newton derivative for different choices of the finite set $\mathcal{M}$ in Section 4. Furthermore, we will argue in Section 6 that H_γ and hence (2.2) is in fact Newton differentiable, thereby guaranteeing local superlinear convergence of the corresponding semismooth Newton method.

To see the relation of (2.2) to (2.1), we first note that the Yosida approximation $(\partial\mathcal{G}^*)_\gamma$ is linked to the Moreau envelope

$$(\mathcal{G}^*)_\gamma(p) = \min_{\tilde p\in U} \frac{1}{2\gamma}\|\tilde p - p\|_U^2 + \mathcal{G}^*(\tilde p) \tag{2.8}$$

via $(\partial\mathcal{G}^*)_\gamma = \partial(\mathcal{G}^*)_\gamma$; see, e.g., [21, Thm. 7.9], which justifies the term *Moreau–Yosida regularization* (of $\mathcal{G}^*$). Furthermore, from [21, Thm. 7.11], we have that

$$((\mathcal{G}^*)_\gamma)^*(u) = \mathcal{G}(u) + \frac{\gamma}{2}\|u\|_U^2 \tag{2.9}$$

and, hence, (2.7) coincides with the necessary and sufficient optimality conditions for the strictly convex minimization problem

$$\min_{u\in U} \mathcal{E}_\gamma(u) \quad \text{for } \mathcal{E}_\gamma(u) = \mathcal{F}(u) + \mathcal{G}(u) + \frac{\gamma}{2}\|u\|_U^2. \tag{2.10}$$

By the same arguments as in the proof of Proposition 2.1, we obtain the existence of a minimizer $u_\gamma \in U$ and thus of a corresponding $p_\gamma = -\mathcal{F}(u_\gamma) \in U$.

Remark 2.3. An alternative regularization leading to Newton differentiability is to instead apply the Yosida approximation to the equivalent subdifferential inclusion $\bar p \in \partial\mathcal{G}(\bar u)$ in (2.2). This would correspond to replacing $\mathcal{G}$ in (2.1) with its (Fréchet-differentiable) Moreau envelope $\mathcal{G}_\gamma : u \mapsto \min_{\tilde u\in U} \frac{1}{2\gamma}\|\tilde u - u\|_U^2 + \mathcal{G}(\tilde u)$, thus smoothing out the nondifferentiability that is responsible for the structural properties of the penalty. In contrast, our regularization does not remove the nondifferentiability but merely makes the functional (more) strongly convex so that the structural features of the multibang regularization are preserved.

We now address convergence of solutions to (2.10) as $\gamma \to 0$. The following statement is a slight generalization of [18, Prop. 4.1]. We here prove it by Γ-convergence (see [10] for a gentle introduction), which is a classical technique to check whether the solution of a perturbed optimization problem converges, as the perturbation tends to zero, to the solution of the unperturbed problem. The term "perturbation" may here be interpreted in a broad sense; in the subsequent statement it is used in the sense of a so-called singular perturbation (where the optimization problem depends on a small model or regularization parameter that approaches zero), but in the next section it will represent perturbations of the target state or measurement z (and it could for instance just as well represent discretizations of a continuous optimization problem). If a sequence $\mathcal{E}_n$ of energies Γ-converges to some energy $\mathcal{E}$ (which means that for any sequence $u_n \to u$ we have $\mathcal{E}(u) \le \liminf_{n\to\infty} \mathcal{E}_n(u_n)$ and that for every u there exists a so-called recovery sequence $u_n \to u$ with $\limsup_{n\to\infty} \mathcal{E}_n(u_n) \le \mathcal{E}(u)$) and if the $\mathcal{E}_n$ are uniformly coercive (or just boundedness of $\mathcal{E}_n(u_n)$ implies precompactness of the sequence u_n), then minimizers of $\mathcal{E}_n$ are known to converge (up to subsequences) to minimizers of $\mathcal{E}$.

Proposition 2.4 (limit for vanishing regularization). *Let S satisfy (A1). Then it holds that $\Gamma\text{-}\lim_{\gamma\to 0} \mathcal{E}_\gamma = \mathcal{E}$ with respect to weak convergence in U. As a consequence, any sequence u_{γ_n} of global minimizers to (2.10) for $\gamma_n \to 0$ contains a subsequence converging weakly in U to a global minimizer of (2.1). Moreover, this convergence is strong.*

Proof. For the Γ-limit, we first have to show that for any sequence $\gamma_n \to 0$ and any weakly converging sequence $u_n \rightharpoonup u$ we have $\liminf_{\gamma_n\to 0} \mathcal{E}_{\gamma_n}(u_{\gamma_n}) \ge \mathcal{E}(u)$, which is an immediate consequence of the sequential weak lower semicontinuity of $\mathcal{E}$ (shown in the proof of Proposition 2.1) and of $\|\cdot\|_U$. Second, the required recovery sequence is just the constant sequence $u_n = u$. Furthermore, minimizers of $\mathcal{E}_\gamma$ are uniformly bounded in U, since g is infinite outside the convex hull $\operatorname{co}\mathcal{M}$, which together with the Γ-convergence is well-known to imply the weak convergence in U of minimizers of $\mathcal{E}_\gamma$ to minimizers of $\mathcal{E}$. Finally, for such a weakly converging sequence $u_{\gamma_n} \rightharpoonup u$ of minimizers of $\mathcal{E}_{\gamma_n}$ we have

$$\mathcal{E}(u_{\gamma_n}) + \frac{\gamma_n}{2}\|u_{\gamma_n}\|_U^2 \le \mathcal{E}_{\gamma_n}(u) \le \mathcal{E}(u_{\gamma_n}) + \frac{\gamma_n}{2}\|u\|_U^2, \tag{2.11}$$

which implies $\|u\|_U \ge \|u_{\gamma_n}\|_U$ so that the convergence $u_{\gamma_n} \to u$ is actually strong. □

For error estimates of the Moreau–Yosida approximation in terms of γ (as well as of a finite element discretization in the scalar case) under a regularity assumption, we refer to [14].

3 Stability properties of multibang controls

We now discuss stability properties of the controls by exploiting the special structure of the optimality conditions for the multibang control problem. In particular we consider in what sense the controls converge as the target state converges; what can be said about controls with values in $\mathcal{M}$; and when exact controls (which achieve the target state) can be retrieved by the optimization. To keep the notation concise, we set

$$\mathcal{E}^z(u) := \frac{1}{2}\|S(u) - z\|_Y^2 + \int_\Omega g(u(x))\,\mathrm{d}x, \tag{3.1}$$

where $g : \mathbb{R} \to \overline{\mathbb{R}}$ is again proper, convex, and weakly lower semicontinuous with $\operatorname{dom} g = \operatorname{co} \mathcal{M}$.

3.1 Stability with respect to target perturbations

First, we examine how perturbations of the target z influence the minimizer of (2.1). This is for instance of interest if our control problem actually represents an inverse problem, in which the measurement z is typically slightly perturbed by noise. We will see that as z_n converges strongly to z in Y, the corresponding minimizers converge in U in the weak sense. Strong convergence cannot be expected in general due to worst-case scenarios in which the limit minimizer $\bar u$ has a nonempty "singular arc"

$$\mathcal{S}_{\bar u} = \{x \in \Omega : \bar u(x) \notin \mathcal{M}\}, \tag{3.2}$$

i.e., the region in which $\bar u$ does not attain any of the distinguished values $\mathcal{M}$. However, away from that singular arc one obtains strong convergence and, as a consequence, controls in $\mathcal{M}$ even for perturbed targets. In this section we use the following additional assumptions on S (which will be shown to hold for our model forward operators in Section 5):

(A3) $S : U \to Y$ is compact.

(A4) For some Banach space $V \hookleftarrow U$ with $V^* \hookrightarrow L^\infty(\Omega;\mathbb{R}^m)$, we have

$$\lim_{\tilde u \rightharpoonup u \text{ in } U} \|[S'(\tilde u) - S'(u)]^* y\|_{V^*} = 0 \qquad \text{for all } y \in Y.$$

Proposition 3.1 (Γ-convergence of objective functional). *Let $z_n \to z$ in Y and S satisfy (A1). Then with respect to weak convergence in U, we have*

$$\Gamma\text{-}\lim_{n\to\infty} \mathcal{E}^{z_n} = \mathcal{E}^z.$$

Proof. For the lim inf inequality, let $u_n \rightharpoonup u$ weakly in U, then by property (A1) and the weak lower semicontinuity of $\|\cdot\|_Y$ and the convexity of g, we have

$$\begin{aligned}\liminf_{n\to\infty} \mathcal{E}^{z_n}(u_n) &= \liminf_{n\to\infty} \frac{1}{2}\|S(u_n) - z_n\|_Y^2 + \int_\Omega g(u_n(x))\,\mathrm{d}x\\ &\geq \frac{1}{2}\|S(u) - z\|_Y^2 + \int_\Omega g(u(x))\,\mathrm{d}x = \mathcal{E}^z(u).\end{aligned}$$

For the lim sup inequality, choose $u_n = u \in U$ to obtain

$$\limsup_{n\to\infty} \mathcal{E}^{z_n}(u_n) = \limsup_{n\to\infty} \frac{1}{2}\|S(u) - z_n\|_Y^2 + \int_\Omega g(u(x))\,\mathrm{d}x = \mathcal{E}^z(u).$$

□

This proposition now implies a weak stability of the control.

Corollary 3.2 (stability of control and state). *Under the conditions of Proposition 3.1 and (A3), any sequence $\{u_n\}_{n\in\mathbb{N}}$ of minimizers of $\mathcal{E}^{z_n}$ contains a subsequence converging weakly in U to a minimizer $\bar u$ of $\mathcal{E}^z$. The corresponding states $y_n = S(u_n)$ converge strongly in Y to $\bar y = S(\bar u)$.*

Proof. Since g is infinite outside co $\mathcal{M}$ we know that $\|u\|_{L^\infty(\Omega;\mathbb{R}^n)}$ is uniformly bounded among all $u \in U$ with finite energy $\mathcal{E}^{z_n}(u)$, where the bound is independent of n. Thus, the $\mathcal{E}^{z_n}$ are equimildly coercive so that the convergence of minimizers u_n follows from the Γ-convergence of the functionals. The convergence of states $y_n = S(u_n) \to \bar y = S(\bar u)$ along the subsequence follows from $u_n \rightharpoonup \bar u$ together with properties (A1) and (A3) (weak-to-weak continuity and compactness of S, respectively). □

Under additional assumptions, we also obtain convergence of the dual variable.

Corollary 3.3 (stability of dual). *Under the conditions of Proposition 3.1 and (A1)–(A4), consider the sequence of minimization problems $\min_{u\in U} \mathcal{E}^{z_n}(u)$. The corresponding optimal controls u_n, states y_n, and dual variables p_n satisfy up to a subsequence*

$$u_n \rightharpoonup \bar u \text{ in } U, \quad y_n \to \bar y \text{ in } Y, \quad \text{and} \quad p_n \to \bar p \text{ in } V^*,$$

where $\bar u$ is a minimizer of $\mathcal{E}^z$, $\bar y = S(\bar u)$, and $\bar p$ satisfies (2.2).

Proof. We already know $u_n \rightharpoonup \bar u$ and $y_n \to \bar y$. By the Banach–Steinhaus theorem and (A4), $[S'(u_n) - S'(\bar u)]^*$ is uniformly bounded in $L(Y;V^*)$ and thus also $S'(u_n)^*$. Now

$$\begin{aligned}\|p_n - \bar p\|_{V^*} &= \|S'(u_n)^*(z_n - y_n) - S'(\bar u)^*(z - \bar y)\|_{V^*}\\ &\le \|S'(u_n)^*(z_n - y_n) - S'(u_n)^*(z - \bar y)\|_{V^*} + \|S'(u_n)^*(z - \bar y) - S'(\bar u)^*(z - \bar y)\|_{V^*}\\ &\le \|S'(u_n)^*\|_{L(Y;V^*)}\|z_n - y_n - (z - \bar y)\|_Y + \|[S'(u_n)^* - S'(\bar u)^*](z - \bar y)\|_{V^*} \to 0.\end{aligned} \tag{3.3}$$

□

The final result shows strong convergence of controls outside the singular arc, which will be seen to correspond to the case where $\partial g^*(\bar p(x))$ is set valued (cf. (4.7) and (4.11)).

Proposition 3.4 (locally strong convergence of control). *Let the conditions of Proposition 3.1 and (A1)–(A4) hold. Furthermore, let Q be the set on which ∂g^* is single valued, and abbreviate $\Omega_P = \{x \in \Omega : p(x) \in P\}$ for given $P \subset \mathbb{R}^m$. Then we have*

(i) for any $P \subset\subset Q$ compact and n large enough, $u_n(x) = \bar u(x) \in \mathcal{M}$ for a.e. $x \in \Omega_P$;

(ii) $u_n|_{\Omega_Q} \to \bar u|_{\Omega_Q}$ strongly in $L^2(\Omega_Q;\mathbb{R}^m)$ and $\bar u(x) \in \mathcal{M}$ for a.e. $x \in \Omega_Q$.

Proof. By Corollary 3.3, we have $p_n \to \bar p$ in $L^\infty(\Omega;\mathbb{R}^m)$. In particular, for n large enough, for all $x \in \Omega_P$ the value $p_n(x)$ lies in the same connected component of Q as $\bar p(x)$. Hence, $u_n(x) = \bar u(x)$ due to $u_n(x) \in \partial g^*(p_n(x)) = \partial g^*(\bar p(x))$ and $\bar u(x) \in \partial g^*(\bar p(x))$. Since this holds for any compact subset P of Q, we actually have pointwise convergence $u_n(x) \to \bar u(x)$ for almost all $x \in \Omega_Q$. The uniform boundedness of u_n (since otherwise $g(u_n(x)) = \infty$) then implies strong convergence by the dominated convergence theorem. □

3.2 controls in $\mathcal{M}$

Here, we examine more closely controls taking values only in $\mathcal{M}$. In the following, we refer to minimizers $\bar u \in U$ of $\mathcal{E}^z$ with $\bar u(x) \in \mathcal{M}$ for almost everywhere $x \in \Omega$ as *multibang controls*. First, we note that such controls allow us to achieve an energy arbitrarily close to the optimum.

Remark 3.5 (near-optimality). Under assumptions (A1) and (A3), we have

$$\min_{u\in U} \mathcal{E}^z(u) = \inf_{\substack{u\in U\\ u(x)\in\mathcal{M}\text{ a.e.}}} \mathcal{E}^z(u).$$

Indeed, let $\bar u \in U$ minimize $\mathcal{E}^z$. By the definition of g, there exists a sequence $\{u_n\}_{n\in\mathbb{N}} \subset U$ with $u_n(x) \in \mathcal{M}$ a.e., $u_n \rightharpoonup \bar u$ in U, and $\int_\Omega g(u_n(x))\,\mathrm{d}x \to \int_\Omega g(\bar u(x))\,\mathrm{d}x$. Furthermore, $S(u_n) \to S(\bar u)$ in Y so that $\mathcal{E}^z(u_n) \to \mathcal{E}^z(\bar u)$.

In the remainder of this subsection, we shall restrict ourselves to the case that

(a5) $S : U \to Y$ is linear,

which will only apply to the elasticity example, but not to the Bloch setting. The intuition is that the case with multibang controls is generic (or even that targets with nonmultibang controls, i.e., $u(x) \notin \mathcal{M}$ on a nonnegligible set, are nowhere dense in Y). This is consistent with Proposition 3.4, since targets with a singular arc of zero measure (or rather with $\Omega_Q = \Omega$) can be perturbed without producing a singular arc. Below we will at least see that targets leading to multibang controls are dense in Y; and that the mapping $z \mapsto \arg\min_{u\in U} \mathcal{E}^z(u)$ is not continuous in any target z for which the singular arc has positive measure.

Proposition 3.6 (approximation via multibang control). *Let S satisfy (A1)–(a5). Then for any $z \in Y$ and corresponding minimizer $\bar u \in U$ of $\mathcal{E}^z$, there exists a sequence $\{z_n\}_{n\in\mathbb{N}} \subset Y$ with $z_n \to z$ such that the corresponding minimizers $u_n \in U$ of $\mathcal{E}^{z_n}$ satisfy $u_n(x) \in \mathcal{M}$ almost everywhere, $u_n \rightharpoonup \bar u$, and $\mathcal{E}^{z_n}(u_n) = \mathcal{E}^z(\bar u)$.*

Sketch of proof. By (2.2), we have $\bar p = S^*(z - S\bar u)$ and $\bar u(x) \in \partial g^*(\bar p(x))$ for almost all $x \in \Omega$. The piecewise affine structure of $g^* : \mathbb{R}^m \to \mathbb{R}$ implies that $\bar u(x)$ is a convex combination of (at most) $m+1$ values $\hat u_j \in \mathcal{M}\cap\partial g^*(\bar p(x))$. Thus one can find $u_n \rightharpoonup \bar u$ with $u_n(x) \in \mathcal{M}\cap\partial g^*(\bar p(x))$ for almost all $x \in \Omega$. Choosing $z_n = Su_n + (z - S\bar u)$, we have $z_n \to z$ as well as $\bar p = S^*(z_n - Su_n)$ and $u_n(x) \in \partial g^*(\bar p(x))$ for almost all $x \in \Omega$. Hence by the convexity of the energy $\mathcal{E}^{z_n}$, u_n is a minimizer of $\mathcal{E}^{z_n}$. Furthermore, one can even choose u_n such that $\int_\Omega g(u_n(x))\,\mathrm{d}x = \int_\Omega g(\bar u(x))\,\mathrm{d}x$ so that $\mathcal{E}^{z_n}(u_n) = \mathcal{E}^z(\bar u)$ as claimed. □

Corollary 3.7 (strong convergence of control). *Let the conditions of Proposition 3.6 hold. Then*

(i) the targets z admitting a multibang control $\bar u$ minimizing $\mathcal{E}^z$ are dense in Y;

(ii) if S is injective and the minimizer $\bar u$ to $\mathcal{E}^z$ has a singular arc of positive measure, then one cannot have strong convergence of minimizers u_n of $\mathcal{E}^{z_n}$ for all $z_n \to z$.

Proof. The first statement is a direct consequence of Proposition 3.6. The second statement follows from the strict convexity of $\mathcal{E}^z$ and thus the uniqueness of its minimizers, together with the fact that strong convergence in U implies pointwise convergence: Indeed, let $\bar u$ have a singular arc $\mathcal{S}_{\bar u}$ of positive measure and choose $z_n \to z$ such that the unique minimizers u_n of $\mathcal{E}^{z_n}$ are multibang controls (which is possible by the first statement). If we had strong convergence $u_n \to \bar u$ in U, then (up to a subsequence) also $u_n \to \bar u$ pointwise almost everywhere, in particular, on $\mathcal{S}_{\bar u}$. This contradicts $u_n(x) \in \mathcal{M}$ almost everywhere. □

3.3 RETRIEVAL OF EXACT CONTROLS

We now consider more specifically the consequence of the convex relaxation (1.2) for some nonnegative and strictly convex $c : \mathbb{R}^m \to \mathbb{R}$. A peculiar feature of the multibang control in this case is that for attainable targets, i.e., if there exists a $\hat u \in U$ such that $z = S(\hat u)$, the generating control $\hat u$ can only be recovered as a minimizer $\bar u$ of the optimization problem (2.1) if $c(\hat u(x)) = \min_{v\in\mathcal{M}} c(v)$ almost everywhere. This demonstrates the desirability of allowing multiple admissible control values of equal magnitude.

Proposition 3.8 (achievement of target). *If S satisfies (A2), then, for any minimizer $\bar u \in U$ of $\mathcal{E}^z$ that satisfies $S(\bar u) = z$, it holds that $g(\bar u(x)) = \min_{v\in\mathcal{M}} g(v)$ almost everywhere. In particular, if in addition $\bar u(x) \in \mathcal{M}$ almost everywhere, then $c(\bar u(x)) = \min_{v\in\mathcal{M}} c(v)$.*

Proof. If $S(\bar u) = z$, the first relation in the optimality condition (2.2) together with linearity of $S'(\bar u)$ implies $\bar p = 0$. Hence, the second relation yields $\bar u \in \partial\mathcal{G}^*(0)$ and therefore $0 \in \partial\mathcal{G}(\bar u)$. By (2.3), this implies $0 \in \partial g(\bar u(x))$ for almost all $x \in \Omega$ and therefore

$$g(\bar u(x)) = \min_{v\in\mathbb{R}^m} g(v) = \inf_{v\in\mathbb{R}^m} g_\infty(v) = \inf_{v\in\mathcal{M}} \alpha c(v) = \min_{v\in\mathcal{M}} g(v) \tag{3.4}$$

since $\min f^{**} = \inf f$ by the properties of the convex hull; see, e.g., [4, Prop. 12.9 (iii)]. □

If, however, $c(\hat u(x)) = \min_{v\in\mathcal{M}} c(v)$ is not satisfied almost everywhere, then the generating control $\hat u$ can only be recovered in the limit $\alpha \to 0$. In fact, in this limit the best approximation is achieved, i.e., an optimal control which yields the minimum possible tracking term $\mathcal{F}$. In the following, we denote by u_α the minimizer of $\mathcal{E}^z$ (which depends on α via the definition (1.2) of g) for given $\alpha > 0$.

Proposition 3.9 (Γ-convergence for vanishing regularization). *For given $z \in Y$, let $M := \inf_{u\in U} \|S(u) - z\|_Y$ and $O := \{u \in U : \|S(u) - z\|_Y = M\}$. If S satisfies (A1), then with respect to weak convergence in U we have*

$$\Gamma\text{-}\lim_{\alpha\to 0} \frac{1}{\alpha}\left(\mathcal{E}^z - \frac{M^2}{2}\right) = \delta_O + \mathcal{G}_1, \tag{3.5}$$

where

$$\mathcal{G}_1(u) = \int_\Omega g_1^{**}(u(x))\,\mathrm{d}x \quad \text{for} \quad g_1(u) = c(u) + \delta_\mathcal{M}(u). \tag{3.6}$$

Proof. The lim sup inequality is trivial using the constant sequence; for the lim inf inequality we only have to consider a sequence $u_\alpha \rightharpoonup u \notin O$. In that case,

$$\liminf_{\alpha\to 0} \|S(u_\alpha) - z\|_Y \geq \|S(u) - z\|_Y > M \tag{3.7}$$

so that

$$\frac{1}{\alpha}\left(\min_{u\in U} \frac{1}{2}\|S(u) - z\|_Y^2 + \int_\Omega g(u(x))\,\mathrm{d}x - \frac{M^2}{2}\right) \to \infty.$$

□

Corollary 3.10 (approximation of target). *Under the conditions of the previous proposition, if $O \neq \emptyset$, then any family $\{u_\alpha\}_{\alpha>0}$ of minimizers of $\mathcal{E}^z$ contains a subsequence converging weakly to a minimizer $\bar u \in O$ of $\mathcal{G}_1$.*

Proof. This follows from the equimild coerciveness of the energies and the Γ-convergence; see [10, Def. 1.19 and Thm. 1.21]. □

4 Vector-valued multibang penalty

To implement the general framework of Section 2, we need explicit characterizations of the Fenchel conjugate and its subdifferential as well as its Moreau–Yosida regularization for the multibang penalty (1.2). Recall that $\mathcal{G}$ is defined as an integral functional for the proper, convex, and lower semicontinuous integrand

$$g = (\alpha c(\cdot) + \delta_\mathcal{M})^{**} = g_\infty^{**}. \tag{4.1}$$

We can thus proceed by pointwise computation.

We first summarize the general procedure. Since $g^* = (g_\infty^{**})^* = (g_\infty^*)^{**} = g_\infty^*$, the Fenchel conjugate of g is given by

$$g^*(q) = g_\infty^*(q) \coloneqq \sup_{v\in\mathbb{R}^m} \langle v, q\rangle - g_\infty(v) = \max_{v\in\mathcal{M}} \langle v, q\rangle - \alpha c(v). \tag{4.2}$$

Hence, g^* is the maximum of a finite number of convex and continuous functions of q, and we can thus compute its subdifferential (without computing g^* first!) using the maximum rule; see, e.g., [44, Prop. 4.5.2, Rem. 4.5.3]. Setting

$$g_v^*(q) \coloneqq \langle v, q\rangle - \alpha c(v),$$

we have

$$\partial g^*(q) = \operatorname{co} \bigcup_{\substack{v\in\mathcal{M}:\\ g^*(q)=g_v^*(q)}} \partial g_v^*(q) = \operatorname{co}\left\{v \in \mathcal{M} : g^*(q) = g_v^*(q)\right\} \tag{4.3}$$

with co denoting the convex hull. Obviously, the subdifferential ∂g^* is piecewise constant. If we denote the elements of $\mathcal{M}$ by $\bar u_i$ for i from some index set I, then ∂g^* takes the value $\operatorname{co}\{\bar u_{i_1}, \dots, \bar u_{i_k}\}$ with $i_1, \dots, i_k \in I$ on

$$Q_{i_1\dots i_k} = \left\{q \in \mathbb{R}^m : g^*(q) = g_{\bar u_i}^*(q) \text{ if and only if } i \in \{i_1, \dots, i_k\}\right\}.$$

For the proximal mapping

$$\operatorname{prox}_{\gamma g^*}(q) \coloneqq \operatorname*{arg\,min}_{w\in\mathbb{R}^m} \frac{1}{2\gamma}|w-q|_2^2 + g^*(w) = (\operatorname{Id}+\gamma\partial g^*)^{-1}(q)$$

we then make use of the equivalence

$$w = (\operatorname{Id}+\gamma\partial g^*)^{-1}(q) \qquad \Leftrightarrow \qquad q \in (\operatorname{Id}+\gamma\partial g^*)(w) = \{w\} + \gamma\partial g^*(w) \tag{4.4}$$

and follow the case distinction in the maximum rule (4.3). In detail, we first define $Q_{i_1\dots i_k}^\gamma$ to be the image of $Q_{i_1\dots i_k}$ under $(\operatorname{Id}+\gamma\partial g^*)$,

$$Q_{i_1\dots i_k}^\gamma = (\operatorname{Id}+\gamma\partial g^*)(Q_{i_1\dots i_k}) = Q_{i_1\dots i_k} + \gamma \operatorname{co}\{\bar u_{i_1}, \dots, \bar u_{i_k}\}.$$

The preimage $w \in Q_{i_1\dots i_k}$ of $q \in Q_{i_1\dots i_k}^\gamma$ under $(\operatorname{Id}+\gamma\partial g^*)$ is thus obtained by solving the linear system of equations

$$\begin{aligned} 0 &= g_{\bar u_{i_l}}^*(w) - g_{\bar u_{i_1}}^*(w), \quad l = 2, \dots, k,\\ q &= w + \gamma(\lambda_1 \bar u_{i_1} + \ldots + \lambda_k \bar u_{i_k}),\\ 1 &= \lambda_1 + \ldots + \lambda_k, \end{aligned}$$

for $w \in \mathbb{R}^m$ and the convex combination coefficients $\lambda_1, \dots, \lambda_k \in \mathbb{R}$. Let us express the solution of this system (obtained by inverting the system matrix; if not invertible use the minimum norm solution) as

$$w = A_{i_1\dots i_k} q + b_{i_1\dots i_k}, \quad \lambda_l = A_{i_1\dots i_k;l} q + b_{i_1\dots i_k;l}, \tag{4.5}$$

for some $A_{i_1\dots i_k} \in \mathbb{R}^{m\times m}$, $b_{i_1\dots i_k} \in \mathbb{R}^m$ and $A_{i_1\dots i_k;l} \in \mathbb{R}^{1\times m}$, $b_{i_1\dots i_k;l} \in \mathbb{R}$, $l = 1, \dots, k$. The Moreau–Yosida regularization $h_\gamma = (\partial g^*)_\gamma$ of ∂g^* is then given by

$$h_\gamma(q) = (\partial g^*)_\gamma(q) = \tfrac{1}{\gamma}\left(q - \operatorname{prox}_{\gamma g^*}(q)\right) = \tfrac{1}{\gamma}(q - A_{i_1\dots i_k} q - b_{i_1\dots i_k}). \tag{4.6}$$

Since $h_\gamma = (\partial g^*)_\gamma$ is continuous and piecewise continuously differentiable (PC^1), its Clarke subdifferential (2.4) at $q \in \mathbb{R}^m$ is given by the convex hull of the derivatives of the branches active at q; see, e.g., [21, Thm. 14.7]. We can thus take as a Newton derivative

$$D_N h_\gamma(q) = \tfrac{1}{\gamma}(\mathrm{Id} - A_{i_1\dots i_k}).$$

To compute $h_\gamma(q)$ and $D_N h_\gamma(q)$ for an arbitrary $q \in \mathbb{R}^m$ it remains to identify the set $Q^\gamma_{i_1\dots i_k}$ in which q lies. To this end, note that $q \in Q^\gamma_{i_1\dots i_k}$ if and only if

$$\begin{aligned}\lambda_l &= A_{i_1\dots i_k;l}\, q + b_{i_1\dots i_k;l} \in [0,1] \quad \text{for } l = 1,\dots,k \quad \text{and}\\ w &= A_{i_1\dots i_k} q + b_{i_1\dots i_k} \in Q_{i_1\dots i_k},\end{aligned}$$

since w represents the preimage of q under $(\mathrm{Id} + \gamma\partial g^*)$ and $\lambda_1,\dots,\lambda_k$ represent the convex combination coefficients such that $w + \lambda_1 \bar u_{i_1} + \ldots + \lambda_k \bar u_{i_k} = q$. To check the condition $w \in Q_{i_1\dots i_k}$ it suffices to check that there is no $i \notin \{i_1,\dots,i_k\}$ with $g^*_{\bar u_i}(w) \geq g^*_{\bar u_{i_1}}(w)$.

Sections 4.1 and 4.2 make this calculation explicit for the first two choices of $\mathcal{M}$ introduced in the introduction and the quadratic cost $c(v) = \frac{1}{2}|v|_2^2$, which is particularly useful for generating more efficient code. We finally address in Section 4.3 the algorithmic evaluation in the general case as relevant for the multimaterial branched transport example.

4.1 RADIALLY DISTRIBUTED CONTROL VALUES

Here, we take as set $\mathcal{M} \subset \mathbb{R}^2$ of admissible control values the vector 0 together with vectors of fixed amplitude $\omega_0 > 0$ and $M > 2$ equidistributed phases

$$0 \leq \theta_1 < \cdots < \theta_M < 2\pi$$

(where we shall assume $\theta_{i+1} - \theta_i < \pi$ for $i = 1,\dots,M-1$ and $\theta_1 - (\theta_M - 2\pi) < \pi$), that is,

$$\mathcal{M} = \left\{ \begin{pmatrix}0\\0\end{pmatrix}, \begin{pmatrix}\omega_0 \cos\theta_1\\ \omega_0 \sin\theta_1\end{pmatrix}, \dots, \begin{pmatrix}\omega_0\cos\theta_M\\ \omega_0 \sin\theta_M\end{pmatrix} \right\} =: \{\bar u_0, \bar u_1, \dots \bar u_M\}.$$

In the following it will be helpful to identify an angle $\theta \in [0, 2\pi)$ with the corresponding point $\vec\theta = (\cos\theta, \sin\theta)$ on the unit circle S^1. Let φ_i denote the midpoint between θ_i and θ_{i+1} (identifying $\theta_{M+1} = \theta_1$ for simplicity), that is, $\vec\varphi_i = (\vec\theta_i + \vec\theta_{i+1})/|\vec\theta_i + \vec\theta_{i+1}|_2$, and introduce the circular sectors

$$C_i = \left\{ \omega\vec\theta \in \mathbb{R}^2 : \theta \in (\varphi_i, \varphi_{i+1}),\ \omega \geq 0 \right\}.$$

Here, $\theta \in (\varphi_i, \varphi_{i+1})$ is to be understood 2π-periodically, that is, φ_{M+1} is identified with φ_1, and $(\varphi_i, \varphi_{i+1})$ with $\varphi_{i+1} < \varphi_i$ is interpreted as $(\varphi_i, \varphi_{i+1} + 2\pi)$.

Fenchel conjugate Using the equivalence of angles and sectors introduced above, it is straightforward to see

$$\langle q, \bar u_i\rangle \geq \langle q, \bar u_j\rangle \quad \text{for all } q \in \overline{C_i},\ j \neq 0.$$

Thus, inserting the concrete choice of $\mathcal{M}$ into (4.2), we obtain

$$g^*(q) = \begin{cases} 0 & \text{if } \langle q, \bar u_i\rangle \leq \frac{\alpha}{2}\omega_0^2 \text{ for all } 1 \leq i \leq M,\\ \langle q, \bar u_i\rangle - \frac{\alpha}{2}\omega_0^2 & \text{if } q \in \overline{C_i} \text{ and } \langle q, \bar u_i\rangle \geq \frac{\alpha}{2}\omega_0^2. \end{cases}$$

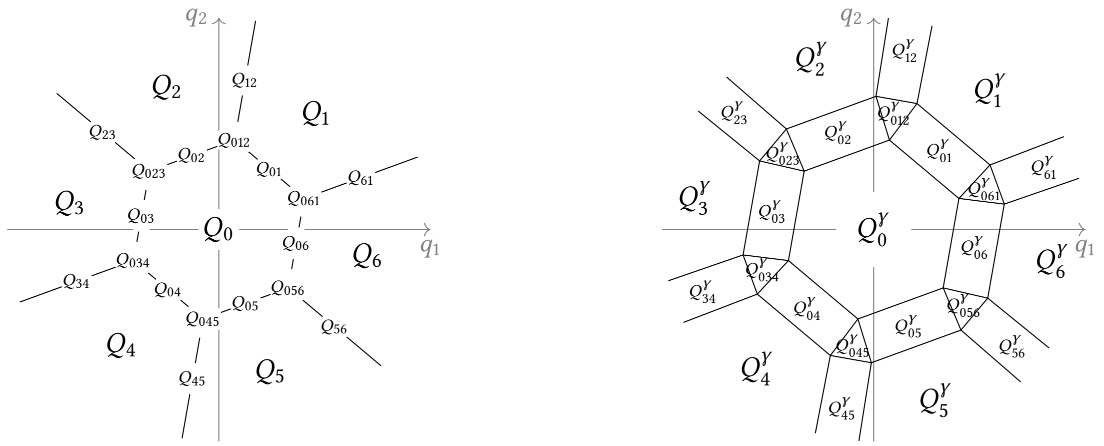

(a) subgradient ∂g^* (b) Moreau–Yosida regularization $(\partial g^*)_\gamma$

Figure 1: Subdomains for radially distributed $\mathcal{M}$

Let us therefore introduce the sets (cf. Figure 1a)

$$
\begin{aligned}
Q_0 &:= \left\{q \in \mathbb{R}^2 : \langle q, \bar u_i\rangle < \tfrac{\alpha}{2}\omega_0^2 \text{ for all } 1 \le i \le M\right\}, && \\
Q_i &:= \left\{q \in C_i : \langle q, \bar u_i\rangle > \tfrac{\alpha}{2}\omega_0^2\right\}, && 1 \le i \le M,\\
Q_{i_1\dots i_k} &:= \bigcap_{i\in\{i_1,\dots,i_k\}} \overline{Q_i} \setminus \bigcup_{i\notin\{i_1,\dots,i_k\}} \overline{Q_i}, && 0 \le i_1,\dots,i_k \le M.
\end{aligned}
$$

With this notation we obtain

$$
g^*(q) = \begin{cases} 0 & \text{if } q \in \overline{Q_0},\\ \langle q, \bar u_i\rangle - \frac{\alpha}{2}\omega_0^2 & \text{if } q \in \overline{Q_i}, \quad 1 \le i \le M.\end{cases}
$$

Subdifferential From the maximum rule (4.3), we directly obtain

$$
\partial g^*(q) = \begin{cases} \{\bar u_i\} & \text{if } q \in Q_i, \qquad 0 \le i \le M,\\ \operatorname{co}\{\bar u_{i_1},\dots,\bar u_{i_k}\} & \text{if } q \in Q_{i_1\dots i_k}, \quad 0 \le i_1,\dots,i_k \le M.\end{cases} \tag{4.7}
$$

Proximal mapping Here, we proceed as follows: For each $Q_{i_1\dots i_k}$, we

1. compute the set $Q^\gamma_{i_1\dots i_k} := (\mathrm{Id} + \gamma\partial g^*)(Q_{i_1\dots i_k})$;
2. solve for $w \in Q_{i_1\dots i_k}$ the relation $q \in \{w\} + \gamma\partial g^*(w)$ for arbitrary $q \in Q^\gamma_{i_1\dots i_k}$.

By (4.4), we then have $w = \operatorname{prox}_{\gamma g^*}(q)$. The details are provided in Table 1, while the sets $Q^\gamma_{i_1\dots i_k}$ are visualized in Figure 1b.

To explain the case $Q_{0,i}$, note that for $q \in Q^\gamma_{0,i}$ we must have by definition of the set $Q^\gamma_{0,i}$ that

$$
(\mathrm{Id} + \gamma\partial g^*)^{-1}(q) = q - \lambda\bar u_i \in Q_{0,i} \subset \left\{v \in \mathbb{R}^2 : \langle v, \bar u_i\rangle = \frac{\alpha}{2}\omega_0^2\right\}
$$

for an appropriate choice of $\lambda \in [0,\gamma]$. Thus,

$$
\langle q - \lambda\bar u_i, \bar u_i\rangle = \tfrac{\alpha}{2}\omega_0^2 \quad \text{and so} \quad \lambda = \frac{\langle q, \bar u_i\rangle}{\omega_0^2} - \frac{\alpha}{2}.
$$

Table 1: Computation of proximal map for radially distributed control values ($i+1$ is to be understood modulo M)

$Q_{i_1\dots i_k}$	$(\mathrm{Id}+\gamma\partial g^*)(w)$	$Q^\gamma_{i_1\dots i_k}$	$(\mathrm{Id}+\gamma\partial g^*)^{-1}(q)$
Q_0	w	Q_0	q
Q_i	$w+\gamma\bar u_i$	$Q_i+\gamma\bar u_i$	$q-\gamma\bar u_i$
$Q_{0,i}$	$w+\gamma\operatorname{co}\{0,\bar u_i\}$	$Q_{0,i}+[0,\gamma]\bar u_i$	$q-\left(\frac{\langle q,\bar u_i\rangle}{\omega_0^2}-\frac{\alpha}{2}\right)\bar u_i$
$Q_{i,i+1}$	$w+\gamma\operatorname{co}\{\bar u_i,\bar u_{i+1}\}$	$Q_{i,i+1}+\gamma\operatorname{co}\{\bar u_i,\bar u_{i+1}\}$	$q-\frac{\gamma(\bar u_i+\bar u_{i+1})}{2}-\frac{\langle q,\bar u_i-\bar u_{i+1}\rangle(\bar u_i-\bar u_{i+1})}{\lvert\bar u_i-\bar u_{i+1}\rvert_2^2}$
$Q_{0,i,i+1}$	$w+\gamma\operatorname{co}\{0,\bar u_i,\bar u_{i+1}\}$	$Q_{0,i,i+1}+\gamma\operatorname{co}\{0,\bar u_i,\bar u_{i+1}\}$	$\alpha\left(\frac{\omega_0}{\lvert\bar u_i+\bar u_{i+1}\rvert_2}\right)^2(\bar u_i+\bar u_{i+1})$

Likewise, for $q\in Q^\gamma_{i,i+1}$ we must have

$$(\mathrm{Id}+\gamma\partial g^*)^{-1}(q)=q-\lambda\bar u_i-(\gamma-\lambda)\bar u_{i+1}\in Q_{i,i+1}\subset(\bar u_i-\bar u_{i+1})^\perp$$

for some $\lambda\in[0,\gamma]$. Thus,

$$0=\langle q-\lambda\bar u_i-(\gamma-\lambda)\bar u_{i+1},\bar u_i-\bar u_{i+1}\rangle=\langle q,\bar u_i-\bar u_{i+1}\rangle+(\tfrac{\gamma}{2}-\lambda)\lvert\bar u_i-\bar u_{i+1}\rvert_2^2$$

and so

$$\lambda=\frac{\gamma}{2}+\frac{\langle q,\bar u_i-\bar u_{i+1}\rangle}{\lvert\bar u_i-\bar u_{i+1}\rvert_2^2}.$$

Finally, note that $Q_{0,i,i+1}=\{\alpha(\frac{\omega_0}{\lvert\bar u_i+\bar u_{i+1}\rvert_2})^2(\bar u_i+\bar u_{i+1})\}$ only contains a single element, which must therefore be equal to $(\mathrm{Id}+\gamma\partial g^*)^{-1}(q)$ for all $q\in Q^\gamma_{0,i,i+1}$.

Moreau–Yosida regularization Inserting the above into definition (4.6) of the Moreau–Yosida regularization yields

$$(\partial g^*)_\gamma(q)=\begin{cases}0 & \text{if } q\in Q_0^\gamma,\\ \bar u_i & \text{if } q\in Q_i^\gamma,\\ \left(\frac{\langle q,\bar u_i\rangle}{\gamma\omega_0^2}-\frac{\alpha}{2\gamma}\right)\bar u_i & \text{if } q\in Q^\gamma_{0,i},\\ \frac{\bar u_i+\bar u_{i+1}}{2}+\frac{\langle q,\bar u_i-\bar u_{i+1}\rangle(\bar u_i-\bar u_{i+1})}{\gamma\lvert\bar u_i-\bar u_{i+1}\rvert_2^2} & \text{if } q\in Q^\gamma_{i,i+1},\\ \frac{q}{\gamma}-\frac{\alpha}{\gamma}\left(\frac{\omega_0}{\lvert\bar u_i+\bar u_{i+1}\rvert_2}\right)^2(\bar u_i+\bar u_{i+1}) & \text{if } q\in Q^\gamma_{0,i,i+1}.\end{cases}\tag{4.8}$$

Finally, in a numerical implementation it will be necessary to efficiently identify for a given $q\in\mathbb{R}^2$ the set $Q^\gamma_{i_1\dots i_k}$ in which it is contained. To this end, determine $i_q,j_q,k_q\in\{1,\dots,M\}$ via

$$q\in\overline{C_{i_q}},\qquad q-\gamma\bar u_{i_q}\in\overline{C_{j_q}},\qquad q-\left(\frac{\langle q,\bar u_{i_q}\rangle}{\omega_0^2}-\frac{\alpha}{2}\right)\bar u_{i_q}\in\overline{C_{k_q}},$$

and set

$$\rho_q:=\langle q,\bar u_{i_q}\rangle,\qquad \sigma_q:=\langle q-\tfrac{\gamma}{2}(\bar u_{i_q}+\bar u_{j_q}),\bar u_{i_q}+\bar u_{j_q}\rangle.$$

Now it is straightforward to identify the correct subdomain via

$$\begin{aligned}Q_0^\gamma&=\left\{q\in\mathbb{R}^2:\rho_q<\tfrac{\alpha}{2}\omega_0^2\right\},\\ Q_i^\gamma&=\left\{q\in\mathbb{R}^2:\rho_q>(\tfrac{\alpha}{2}+\gamma)\omega_0^2,\ i_q=i,\ j_q=i\right\},\\ Q^\gamma_{0,i}&=\left\{q\in\mathbb{R}^2:\tfrac{\alpha}{2}\omega_0^2\le\rho_q\le(\tfrac{\alpha}{2}+\gamma)\omega_0^2,\ i_q=i,\ k_q=i\right\},\\ Q^\gamma_{i,i+1}&=\left\{q\in\mathbb{R}^2:\{i,i+1\}=\{i_q,j_q\},\ \sigma_q>\alpha\omega_0^2\right\},\\ Q^\gamma_{0,i,i+1}&=\left\{q\in\mathbb{R}^2:\{i,i+1\}=\{i_q,i_q+\operatorname{sign}(\bar u_{i_q}\times q)\},\ k_q\neq i_q,\ \sigma_q\le\alpha\omega_0^2\right\}.\end{aligned}$$

Newton derivative We can take as a Newton derivative of (4.8) at q any element of the convex hull of the derivatives of the branches active at q; we choose here

$$D_N h_\gamma(q) = \begin{cases} 0 & \text{if } q \in Q_i^\gamma, \\ \frac{1}{\gamma\omega_0^2}\bar{u}_i\bar{u}_i^T & \text{if } q \in Q_{0,i}^\gamma, \\ \frac{1}{\gamma|\bar{u}_i-\bar{u}_{i+1}|_2^2}(\bar{u}_i-\bar{u}_{i+1})(\bar{u}_i-\bar{u}_{i+1})^T & \text{if } q \in Q_{i,i+1}^\gamma, \\ \frac{1}{\gamma}\,\mathrm{Id} & \text{if } q \in Q_{0,i,i+1}^\gamma. \end{cases} \tag{4.9}$$

4.2 CONCENTRIC CORNERS

We now address the case of admissible control values of different magnitudes, where we consider for the sake of an example the concrete set

$$\begin{aligned} \mathcal{M} &= \left\{\begin{pmatrix}1\\1\end{pmatrix}, \begin{pmatrix}1\\-1\end{pmatrix}, \begin{pmatrix}-1\\1\end{pmatrix}, \begin{pmatrix}-1\\-1\end{pmatrix}, \begin{pmatrix}2\\2\end{pmatrix}, \begin{pmatrix}2\\-2\end{pmatrix}, \begin{pmatrix}-2\\2\end{pmatrix}, \begin{pmatrix}-2\\-2\end{pmatrix}\right\} \\ &= \left\{\bar{u}^1_{1,1}, \bar{u}^1_{1,-1}, \bar{u}^1_{-1,1}, \bar{u}^1_{-1,-1}, \bar{u}^2_{1,1}, \bar{u}^2_{1,-1}, \bar{u}^2_{-1,1}, \bar{u}^2_{-1,-1}\right\}. \end{aligned} \tag{4.10}$$

Fenchel conjugate Again inserting $\mathcal{M}$ into (4.2), we see that the maximum is attained either by $v = (q_1/|q_1|, q_2/|q_2|)$ or by $v = 2(q_1/|q_1|, q_2/|q_2|)$, where in the case $q_i = 0$ we may define $q_i/|q_i| \in \{-1, 1\}$ arbitrarily. Hence we obtain after some algebraic manipulations

$$g^*(q) = \max\{|q|_1 - \alpha, 2|q|_1 - 4\alpha\} = \begin{cases} |q|_1 - \alpha & \text{if } |q|_1 \le 3\alpha, \\ 2|q|_1 - 4\alpha & \text{if } |q|_1 \ge 3\alpha. \end{cases}$$

Subdifferential From (4.3), we directly obtain

$$\partial g^*(q) = \mathrm{co} \bigcup_{\substack{i\in\{1,2\}:\\ g^*(q)=g_i^*(q)}} \partial g_i^*(q) \quad \text{for} \quad \begin{cases} g_1^*(q) = |q|_1 - \alpha, \\ g_2^*(q) = 2|q|_1 - 4\alpha. \end{cases}$$

In the above we have

$$\partial g_1^*(q) = \begin{pmatrix}\mathrm{sign}(q_1)\\ \mathrm{sign}(q_2)\end{pmatrix}, \qquad \partial g_2^*(q) = 2\begin{pmatrix}\mathrm{sign}(q_1)\\ \mathrm{sign}(q_2)\end{pmatrix},$$

where sign denotes the set-valued sign of convex analysis, i.e., $\mathrm{sign}(0) = [-1, 1]$. Therefore we obtain

$$\partial g^*(q) = \left.\begin{cases} \partial g_1^*(q) & \text{if } |q|_1 < 3\alpha \\ \partial g_2^*(q) & \text{if } |q|_1 > 3\alpha \\ \mathrm{co}\{\partial g_1^*(q), \partial g_2^*(q)\} & \text{if } |q|_1 = 3\alpha \end{cases}\right\} = \begin{pmatrix}\mathrm{sign}(q_1)\\ \mathrm{sign}(q_2)\end{pmatrix} \cdot \begin{cases} 1 & \text{if } |q|_1 < 3\alpha, \\ 2 & \text{if } |q|_1 > 3\alpha, \\ [1,2] & \text{if } |q|_1 = 3\alpha. \end{cases}$$

For economy, let us introduce for $i, j, k \in \{-1, 0, 1\}$ the sets

$$I_k = \begin{cases} (-\infty, 0) & \text{if } k = -1, \\ \{0\} & \text{if } k = 0 \\ (0, \infty), & \text{if } k = 1, \end{cases} \qquad \text{and} \qquad Q_{ijk} = \left\{q \in \mathbb{R}^2 : q_1 \in I_i,\ q_2 \in I_j,\ |q|_1 - 3\alpha \in I_k\right\}.$$

A visualization is given in Figure 2a. Note that the index 0 always indicates a lower-dimensional structure; in particular, we have

$$Q_{0jk} \subset \overline{Q_{-1,j,k}} \cap \overline{Q_{1,j,k}}, \quad Q_{i0k} \subset \overline{Q_{i,-1,k}} \cap \overline{Q_{i,1,k}}, \quad Q_{ij0} \subset \overline{Q_{i,j,-1}} \cap \overline{Q_{i,j,1}}.$$

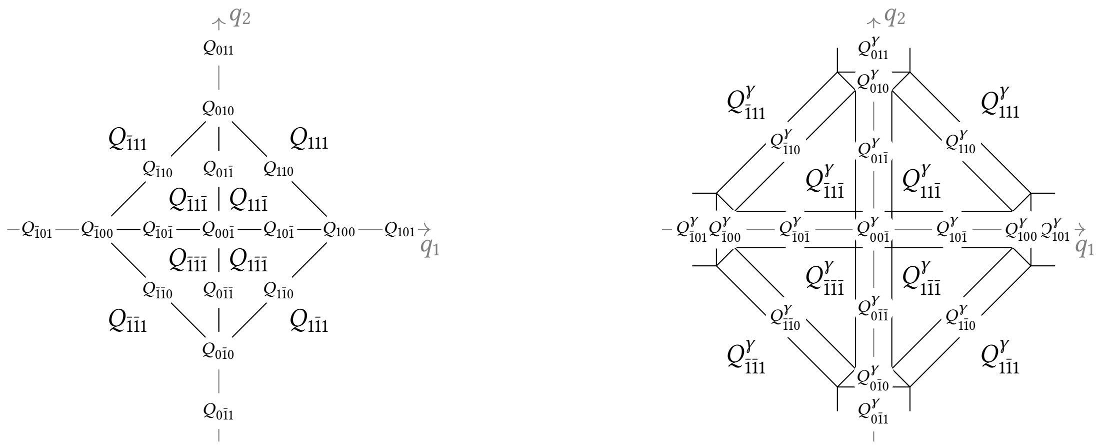

(a) subgradient ∂g^*

(b) Moreau–Yosida regularization $(\partial g^*)_\gamma$

Figure 2: Subdomains for concentric corners, where $\bar{1}$ is written for -1 to simplify notation (the line dimensions are provided in Figure 3)

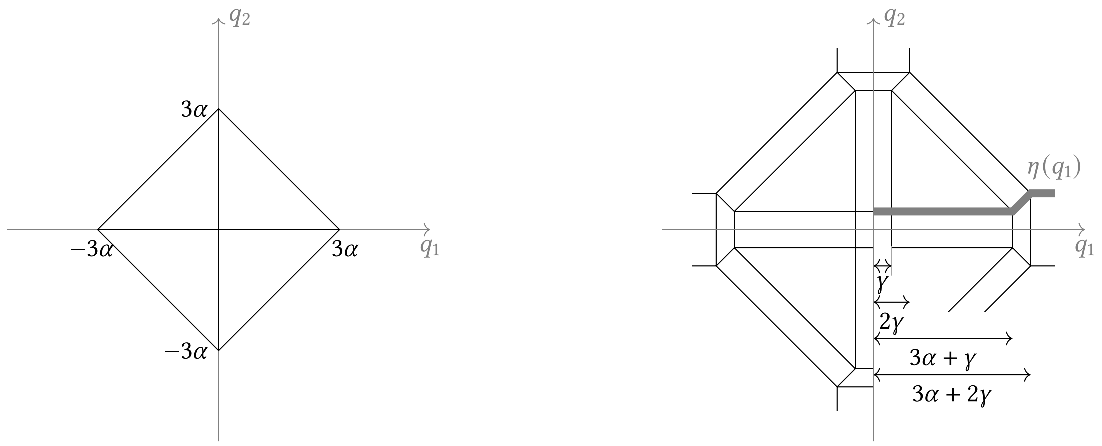

(a) subgradient ∂g^*

(b) Moreau–Yosida regularization $(\partial g^*)_\gamma$

Figure 3: Dimensions for Figure 2

Using this notation, we can write the subdifferential as
(4.11)

$$\partial g^*(q) = \begin{cases} \bar{u}_{ij}^{(k+3)/2} & \text{if } q \in Q_{ijk},\ i,j,k \in \{-1,1\}, \\ \operatorname{co}\left\{\bar{u}_{rs}^{(t+3)/2} : r,s,t \in \{-1,1\},\ |r-i|, |s-j|, |t-k| \leq 1\right\} & \text{if } q \in Q_{ijk},\ 0 \in \{i,j,k\}, \end{cases}$$

which provides more insight into its structure. In particular, on each lower-dimensional Q_{ijk} the subdifferential is the convex hull of the subdifferentials on the adjacent two-dimensional sets.

Proximal mapping To obtain the Moreau–Yosida regularization of ∂g^* for $\gamma > 0$, we proceed as above by first noting that $w = (\operatorname{Id} + \gamma \partial g^*)^{-1}(q) \in Q_{ijk}$ holds if and only if

$$q \in (\operatorname{Id} + \gamma \partial g^*)(Q_{ijk}) =: Q_{ijk}^\gamma.$$

A visualization of these sets is provided in Figure 2b; we postpone their discussion to the end of the section and first calculate the specific value of the proximal mapping based on (4.4) together with the case distinction in the subdifferential.

Let $w \in Q_{ijk}$ and correspondingly $q \in Q^{\gamma}_{ijk}$ for some $i, j, k \in \{-1, 0, 1\}$.

(i) If $i, j, k \in \{-1, 1\}$ we have $(\operatorname{Id} + \gamma\partial g^*)(w) = w + \gamma \bar{u}_{ij}^{(k+3)/2}$ so that

$$(\operatorname{Id} + \gamma\partial g^*)^{-1}(q) = q - \gamma \bar{u}_{ij}^{(k+3)/2} \qquad \text{for } q \in Q^{\gamma}_{ijk} \text{ with } i, j, k \in \{-1, 1\}.$$

(ii) If two of i, j, k are zero, $(\operatorname{Id} + \gamma\partial g^*)^{-1}(q)$ must be the single unique element of Q_{ijk} and thus

$$(\operatorname{Id} + \gamma\partial g^*)^{-1}(q) = \begin{cases} 0 & \text{if } q \in Q^{\gamma}_{0,0,-1}, \\ 3\alpha(i, j) & \text{if } q \in Q^{\gamma}_{i,j,0} \text{ with } i = 0 \text{ or } j = 0. \end{cases}$$

(iii) If $i = 0$ and $j, k \neq 0$, then for $w \in Q_{0jk}$ we have

$$(\operatorname{Id} + \gamma\partial g^*)(w) = w + \gamma \operatorname{co}\left\{\bar{u}_{-1,j}^{(k+3)/2}, \bar{u}_{1,j}^{(k+3)/2}\right\} = w + \gamma\frac{k+3}{2}([-1, 1], j).$$

Thus for $q \in Q^{\gamma}_{0jk}$ we have $(\operatorname{Id} + \gamma\partial g^*)^{-1}(q) = q - \gamma\frac{k+3}{2}(\lambda, j)$, where $\lambda \in [-1, 1]$ is such that $q - \gamma\frac{k+3}{2}(\lambda, j) \in Q_{0jk} \subset \{0\} \times \mathbb{R}$. Therefore $\lambda = \frac{2}{\gamma(k+3)} q_1$ and

$$(\operatorname{Id} + \gamma\partial g^*)^{-1}(q) = \left(0, q_2 - \gamma\tfrac{k+3}{2} j\right) \qquad \text{for } q \in Q^{\gamma}_{0jk} \text{ with } j, k \in \{-1, 1\}.$$

Analogously,

$$(\operatorname{Id} + \gamma\partial g^*)^{-1}(q) = \left(q_1 - \gamma\tfrac{k+3}{2} i, 0\right) \qquad \text{for } q \in Q^{\gamma}_{i0k} \text{ with } i, k \in \{-1, 1\}.$$

(iv) If $k = 0$ and $i, j \neq 0$, then for $w \in Q_{ij0}$ we have

$$(\operatorname{Id} + \gamma\partial g^*)(w) = w + \gamma \operatorname{co}\left\{\bar{u}^1_{ij}, \bar{u}^2_{ij}\right\} = w + \gamma[1, 2](i, j).$$

Thus for $q \in Q^{\gamma}_{ij0}$ we have $(\operatorname{Id} + \gamma\partial g^*)^{-1}(q) = q - \gamma\lambda(i, j)$, where $\lambda \in [1, 2]$ is such that $q - \gamma\lambda(i, j) \in Q_{ij0} \subset \{w \in \mathbb{R}^2 : |w|_1 = 3\alpha\}$. Therefore $\lambda = \frac{|q|_1 - 3\alpha}{2\gamma}$ and

$$(\operatorname{Id} + \gamma\partial g^*)^{-1}(q) = q - \tfrac{|q|_1 - 3\alpha}{2}(i, j) \qquad \text{for } q \in Q^{\gamma}_{ij0} \text{ with } i, j \in \{-1, 1\}.$$

It remains to discuss the sets Q^{γ}_{ijk}. Rather than list all sets explicitly, we instead provide a procedure for determining for a given $q \in \mathbb{R}^2$ the corresponding subdomain, which is what is actually required for the numerical implementation. For that purpose, let us introduce the function (compare the illustration in Figure 3b)

$$\eta(x) = \begin{cases} \gamma & \text{if } x < 3\alpha + \gamma, \\ x - 3\alpha & \text{if } 3\alpha + \gamma \leq x \leq 3\alpha + 2\gamma, \\ 2\gamma & \text{if } x > 3\alpha + 2\gamma. \end{cases}$$

With this function we have $q \in Q^{\gamma}_{ijk}$ for i, j, k given by

$$i = \begin{cases} 0 & \text{if } |q_1| \leq \eta(|q_2|), \\ \operatorname{sign}(q_1) & \text{otherwise}, \end{cases}$$

$$j = \begin{cases} 0 & \text{if } |q_2| \leq \eta(|q_1|), \\ \operatorname{sign}(q_2) & \text{otherwise}, \end{cases}$$

$$k = \begin{cases} -1 & \text{if } |q|_\infty < 3\alpha + \gamma \text{ and } |q|_1 < 3\alpha + 2\gamma, \\ 1 & \text{if } |q|_\infty > 3\alpha + 2\gamma \text{ or } |q|_1 > 3\alpha + 4\gamma, \\ 0 & \text{otherwise}. \end{cases}$$

Moreau–Yosida regularization Inserting this into the definition (4.6) of the Moreau–Yosida regularization yields

$$(\partial g^*)_\gamma(q) = \begin{cases} \bar u_{ij}^{(k+3)/2} & \text{if } q \in Q^\gamma_{ijk} \text{ with } i,j,k \neq 0,\\ \frac{1}{\gamma}(q - 3\alpha(i,j)) & \text{if } q \in Q^\gamma_{ijk} \text{ with } |i|+|j|+|k| = 1,\\ (\frac{1}{\gamma}q_1, \frac{k+3}{2}j) & \text{if } q \in Q^\gamma_{0jk} \text{ with } j,k \neq 0,\\ (\frac{k+3}{2}i, \frac{1}{\gamma}q_2) & \text{if } q \in Q^\gamma_{i0k} \text{ with } i,k \neq 0,\\ \frac{|q|_1 - 3\alpha}{2\gamma}(i,j) & \text{if } q \in Q^\gamma_{ij0} \text{ with } i,j \neq 0. \end{cases} \tag{4.12}$$

Newton derivative Finally, we can again take as a Newton derivative any element of the Clarke gradient; here, we choose

$$D_N h_\gamma(q) = \begin{cases} 0 & \text{if } q \in Q^\gamma_{ijk} \text{ with } i,j,k \neq 0,\\ \frac{1}{\gamma}\,\mathrm{Id} & \text{if } q \in Q^\gamma_{ijk} \text{ with } |i|+|j|+|k| = 1,\\ \frac{1}{\gamma}(j,i)^T(j,i) & \text{if } q \in Q^\gamma_{ijk} \text{ with } |i|+|j| = 1, k \neq 0,\\ \frac{1}{2\gamma}(i,j)^T(i,j) & \text{if } q \in Q^\gamma_{ij0} \text{ with } i,j \neq 0. \end{cases} \tag{4.13}$$

4.3 general multibang control

For more than two control dimensions or arbitrary sets $\mathcal{M}$ an explicit calculation quickly becomes complicated. However, note that $Q_{i_1\dots i_k}$ is actually empty for most index collections $\{i_1,\dots,i_k\}$, so that the number of conditions to be checked in an algorithmic evaluation can be greatly reduced. Indeed, by construction the sets $Q_{i_1\dots i_k}$ are nothing else but the preimages under g^* of the faces of the (polyhedral) graph of g^*. Thus, finding all nonempty $Q_{i_1\dots i_k}$ is equivalent to enumerating all faces of the graph of g^*, which for given choices of c and the $\bar u_i$ can be done by existing face enumeration algorithms such as [28]. Hence the general procedure outlined in the beginning of this section can be implemented for given $\mathcal{M} = \{\bar u_i : i \in I\}$ and c as follows:

1. Use the algorithm from [28] to list all faces of

   $$\operatorname{epi} g^* = \{(q,t) \in \mathbb{R}^{m+1} : t \geq \langle \bar u_i, q\rangle - \alpha c(\bar u_i) \text{ for } i \in I\}.$$

   where a face is identified by the indices $\{i_1,\dots,i_k\} \subset I$ whose constraints are active on that face; these index collections are exactly those for which $Q_{i_1\dots i_k}$ is nonempty.

2. For each face $\mathfrak{f} = \{i_1,\dots,i_k\}$, compute $A_\mathfrak{f}$, $b_\mathfrak{f}$ and $A_{\mathfrak{f};l}$, $b_{\mathfrak{f};l}$ from (4.5).

3. To evaluate h_γ at a vector $q \in \mathbb{R}^m$, calculate $w_\mathfrak{f} = A_\mathfrak{f} q + b_\mathfrak{f}$ and $\lambda_{\mathfrak{f};l} = A_{\mathfrak{f};l} q + b_{\mathfrak{f};l}$ for each face $\mathfrak{f}$. Identify the (unique) face $\mathfrak{f}$ such that $0 \leq \lambda_{\mathfrak{f};l} \leq 1$ for all l and $g_{\bar u_{i_1}}(q) > g_{\bar u_i}(q)$ for $i_1 \in \mathfrak{f}$ and all $i \notin \mathfrak{f}$. Then set

   $$h_\gamma(q) = \frac{1}{\gamma}(q - A_\mathfrak{f} q - b_\mathfrak{f}) \qquad \text{and} \qquad D_N h_\gamma = \frac{1}{\gamma}(\mathrm{Id} - A_\mathfrak{f}).$$

We point out that the computationally most expensive step – enumerating the faces of $\operatorname{epi} g^*$, which requires solving a linear program – is independent of q and γ and can thus be precomputed.

5 state equation

In this section, we specify in more detail our model state operators and verify that assumptions (A1)–(A4) of Sections 2 and 3 are satisfied for our model problems.

5.1 bloch equation

As our motivating model problem, we consider the Bloch equation in a rotating reference frame without relaxation

$$\frac{\mathrm{d}}{\mathrm{d}t}\mathbf{M}^{(\omega)}(t) = \mathbf{M}^{(\omega)}(t) \times \mathbf{B}^{(\omega)}(t), \qquad \mathbf{M}^{(\omega)}(0) = (0,0,1)^T,$$

which describes the temporally evolving magnetization $\mathbf{M}^{(\omega)} \in \mathbb{R}^3$ of an ensemble of spins rotating at the same resonance offset frequency ω (called *isochromat*), starting from a given equilibrium magnetization. The time-varying effective magnetic field $\mathbf{B}^{(\omega)}(t)$ is of the form

$$\mathbf{B}^{(\omega)}(t) = (\omega_x(t), \omega_y(t), \omega)^T,$$

where $u(t) := (\omega_x(t), \omega_y(t)) \in \mathbb{R}^2$ can be controlled. The aim is to achieve a magnetization $\mathbf{M}^{(\omega)}(T) = \mathbf{M}_d$ within the time interval $\Omega = [0,T]$ for a list of offset frequencies $\omega_1, \dots, \omega_J$. In terms of our previous notation we thus set

$$S : L^2(\Omega;\mathbb{R}^2) \to (\mathbb{R}^3)^J, \qquad u \mapsto \left[\mathbf{M}^{(\omega_1)}(T), \dots, \mathbf{M}^{(\omega_J)}(T)\right]. \tag{5.1}$$

This choice of S satisfies the assumptions (a1)–(a4); see Appendix a.

5.2 linear elasticity

In this case, $\Omega \subset \mathbb{R}^2$ represents an elastic body fixed at $\Gamma \subset \partial\Omega$ (with positive Hausdorff measure $\mathcal{H}^1(\Gamma) > 0$), where we assume Γ and $\partial\Omega \setminus \Gamma$ to be smooth or Ω to be a convex polygon with Γ being the union of some faces. The elastic body is subject to a controlled body force $u : \Omega \to \mathbb{R}^2$. The resulting displacement $y : \Omega \to \mathbb{R}^2$ is governed by the equations of linearized elasticity with Lamé parameters μ and λ,

$$\begin{cases} -2\mu \operatorname{div} \epsilon(y) - \lambda \operatorname{grad} \operatorname{div} y = u \text{ in } \Omega, \\ y = 0 \text{ on } \Gamma, \\ (2\mu\epsilon(y) + \lambda \operatorname{div} y)n = 0 \text{ on } \partial\Omega \setminus \Gamma, \end{cases} \tag{5.2}$$

where n denotes the unit outward normal, $Dy = [\nabla y_1 | \nabla y_2]^T$ is the displacement gradient, and $\epsilon(y) = \frac{Dy + Dy^T}{2}$ is the symmetrized gradient. Defining

$$H^1_\Gamma(\Omega) := \left\{ v \in H^1(\Omega;\mathbb{R}^2) : v = 0 \text{ on } \Gamma \right\},$$

we may take

$$S : H^1_\Gamma(\Omega)^* \to H^1_\Gamma(\Omega), \qquad u \mapsto y \text{ solving (5.2)}. \tag{5.3}$$

The solution operator S of the linear elasticity problem is well known to be a bounded linear operator from $U = L^2(\Omega;\mathbb{R}^2)$ into $H^1_\Gamma(\Omega) \hookrightarrow L^2(\Omega;\mathbb{R}^2) =: Y$; see, e.g., [9]. This immediately implies weak-to-weak continuity and Fréchet differentiability with $S'(u) = S$ for all $u \in U$. Similarly, $S'(u)^* = S^*$ for all $u \in U$, and it is readily checked that S is actually self-adjoint so that $S^* = S$. As a consequence we have $\operatorname{ran} S'(u)^* = \operatorname{ran} S \hookrightarrow L^\infty(\Omega;\mathbb{R}^2)$. Indeed, in the case of polygonal domains Ω this follows from $\operatorname{ran} S \subset H^{3/2}(\Omega;\mathbb{R}^2)$ by [41, Thm. 2.3], and in the case of piecewise smooth domains with smooth traction boundary it follows from $\operatorname{ran} S \subset H^2(\Omega;\mathbb{R}^2)$ by [40, Thm. 8]. Summarizing, this choice of S satisfies assumptions (a1)–(a5).

5.3 MULTIMATERIAL BRANCHED TRANSPORT

Here Ω represents a street or pipe network, i.e., a graph that is typically (but not necessarily) embedded in $\mathbb{R}^2$ or $\mathbb{R}^3$. If we assume a constant material flux along the graph edges, the description simplifies to the following: Let $G = (V, E)$ be a directed graph with vertex set V and edge set E representing a transport network. We endow E with the σ-algebra generated by the (finitely many) elements of E and define $L^2(E;\mathbb{R}^m)$ as the space of measurable functions from E to $\mathbb{R}^m$ with the inner product $(u,v)_{L^2} = \sum_{e\in E} \ell(e)u(e)\cdot v(e)$ (where $\ell(e)$ denotes the length of e). The space $L^2(V;\mathbb{R}^m)$ is defined analogously. The function $u \in L^2(E;\mathbb{R}^m)$ describes the flux of m different materials along each edge, and the operator S is the graph divergence, i.e., the difference of outflux and influx at each vertex,

$$S : L^2(E;\mathbb{R}^m) \to L^2(V;\mathbb{R}^m), \quad Su(x) = \sum_{e\in E \text{ incident to } x} u(e) - \sum_{e\in E \text{ emanating from } x} u(e).$$

The target function $z \in L^2(V;\mathbb{R}^m)$ is zero except at the sources and sinks of each material i, where z_i takes the value m_i and $-m_i$, respectively. For this finite-dimensional linear operator S, (A1)–(A5) are automatically fulfilled. Note that an infinite-dimensional setting would likewise be possible; in this case one could choose Ω as the graph embedding and $S : L^2(\Omega;\mathbb{R}^m) \to H^{-s}(\Omega;\mathbb{R}^m)$ with $s > 1$ as the distributional divergence on Ω. Let us also mention that the regularization $\int_\Omega g(u(x))\,\mathrm{d}x$ in the above setting reduces to $\sum_{e\in E} \ell(e)g(u(e))$, which represents the total transport costs.

6 NUMERICAL SOLUTION

We now discuss the numerical solution of the regularized system (2.7) via a semismooth Newton method.

6.1 BLOCH EQUATION

As is usual for time-dependent state equations, we avoid a full space-time discretization by following a reduced approach, i.e., we consider in place of (2.7) the equation

$$u_\gamma - H_\gamma(-\mathcal{F}'(u_\gamma)) = 0. \tag{6.1}$$

Recall that H_γ is a superposition operator defined via

$$[H_\gamma(p)](x) = h_\gamma(p(x)) \qquad \text{for a.e. } x \in \Omega$$

with $h_\gamma = (\partial g^*)_\gamma$ given by (4.8). By Proposition A.3, we have $-\mathcal{F}'(u_\gamma) = S'(u_\gamma)^*(z - S(u_\gamma)) \in L^\infty(\Omega;\mathbb{R}^2)$ and, hence, we can consider $H_\gamma : L^r(\Omega;\mathbb{R}^2) \to L^2(\Omega;\mathbb{R}^2)$ for any $r > 2$. Since h_γ is Lipschitz continuous and piecewise differentiable, semismoothness of H_γ follows from [50, Thm. 3.49] with a Newton derivative given by

$$[D_N H_\gamma(p)h](x) = D_N h_\gamma(p(x))h(x) \qquad \text{for a.e. } x \in \Omega$$

and $D_N h_\gamma$ defined in (4.9).

Further, note that S is twice continuously differentiable. Indeed, this follows by an analogous argument as for Fréchet differentiability in the proof of Proposition A.1: Using the same notation, the second derivative applied to test directions $\varphi, \psi \in L^2(\Omega;\mathbb{R}^2)$ will be given by $S''(u)(\varphi,\psi) = \mathbf{W}(T) = (\mathbf{W}^1(T), \ldots, \mathbf{W}^J(T))$ with

$$\begin{cases} \frac{\mathrm{d}}{\mathrm{d}t}\mathbf{W}^j(t) = B_u^{\omega_j}(t)\mathbf{W}^j(t) + B_\varphi^0(t)\delta\mathbf{M}_\psi^{(\omega_j)}(t) + B_\psi^0(t)\delta\mathbf{M}_\varphi^{(\omega_j)}(t), & t \in [0,T], \\ \mathbf{W}^j(0) = 0, \end{cases}$$

where $S'(u)(\varphi) = (\delta\mathbf{M}_\varphi^{(\omega_1)}(T), \dots, \delta\mathbf{M}_\varphi^{(\omega_J)}(T))$ with $\delta\mathbf{M}_\varphi^{(\omega)}$ satisfying (A.2). This equation has exactly the same structure as (A.2), and thus the argument for showing

$$|S'(\tilde{u})(\varphi) - S'(u)(\varphi) - S''(u)(\tilde{u} - u, \varphi)|_2 = \|\varphi\|_{L^2(\Omega;\mathbb{R}^2)} O(\|\tilde{u} - u\|^2_{L^2(\Omega;\mathbb{R}^2)})$$

works analogously. Since S is twice continuously differentiable, we can apply the chain rule, e.g., from [50, Thm. 3.69], to obtain

$$D_N(H_\gamma \circ (-\mathcal{F}'))(u)\varphi = -D_N H_\gamma(-\mathcal{F}'(u))\mathcal{F}''(u)\varphi$$

for any $\varphi \in L^2(\Omega;\mathbb{R}^2)$. A semismooth Newton step is thus given by $u^{k+1} = u^k + \delta u$, where δu is the solution to

$$\left(\mathrm{Id} + D_N H_\gamma(-\mathcal{F}'(u^k))\mathcal{F}''(u^k)\right)\delta u = -u^k + H_\gamma(-\mathcal{F}'(u^k)), \tag{6.2}$$

which can be obtained, e.g., using a matrix-free Krylov subspace method such as GMRES.

Recall that following Proposition A.2 and [1], $p = -\mathcal{F}'(u)$ can be evaluated by solving the adjoint equations

$$\begin{cases} -\frac{d}{dt}\mathbf{P}^{(\omega_j)}(t) = B_u^\omega(t)\mathbf{P}^{(\omega_j)}(t), & t \in [0, T], \\ \mathbf{P}^{(\omega_j)}(T) = \mathbf{M}_u^{(\omega_j)}(T) - (\mathbf{M}_d)_j \end{cases} \tag{6.3}$$

for $j = 1, \dots, J$ and setting

$$\begin{aligned} p(t) &= \sum_{j=1}^J \begin{pmatrix} \left(\mathbf{M}_u^{(\omega_j)}(t)\right)_3 \mathbf{P}_2^{(\omega_j)}(t) - \left(\mathbf{M}_u^{(\omega_j)}(t)\right)_2 \mathbf{P}_3^{(\omega_j)}(t) \\ \left(\mathbf{M}_u^{(\omega_j)}(t)\right)_3 \mathbf{P}_1^{(\omega_j)}(t) - \left(\mathbf{M}_u^{(\omega_j)}(t)\right)_1 \mathbf{P}_3^{(\omega_j)}(t) \end{pmatrix} \\ &= \sum_{j=1}^J \begin{pmatrix} \mathbf{M}_u^{(\omega_j)}(t)^T B_1 \mathbf{P}^{(\omega_j)}(t) \\ \mathbf{M}_u^{(\omega_j)}(t)^T B_2 \mathbf{P}^{(\omega_j)}(t) \end{pmatrix} \end{aligned}$$

for $t \in [0, T]$, where for the sake of brevity, we have set

$$B_1 := \begin{pmatrix} 0 & 0 & 0 \\ 0 & 0 & -1 \\ 0 & 1 & 0 \end{pmatrix}, \qquad B_2 := \begin{pmatrix} 0 & 0 & -1 \\ 0 & 0 & 0 \\ 1 & 0 & 0 \end{pmatrix}.$$

Similarly, the application of $\mathcal{F}''(u)\varphi$ for given $u, \varphi \in L^2(\Omega;\mathbb{R}^2)$ is given by

$$\mathcal{F}''(u)\varphi = \sum_{j=1}^J \begin{pmatrix} \delta\mathbf{M}_\varphi^{(\omega_j)}(t)^T B_1 \mathbf{P}^{(\omega_j)}(t) + \mathbf{M}_u^{(\omega_j)}(t)^T B_1 \delta\mathbf{P}^{(\omega_j)}(t) \\ \delta\mathbf{M}_\varphi^{(\omega_j)}(t)^T B_2 \mathbf{P}^{(\omega_j)}(t) + \mathbf{M}_u^{(\omega_j)}(t)^T B_2 \delta\mathbf{P}^{(\omega_j)}(t) \end{pmatrix},$$

where $\delta\mathbf{M}_\varphi^{(\omega)}$ (the directional derivative of $\mathbf{M}^{(\omega)}$ with respect to u) is given by the solution of the linearized state equation (A.2) and $\delta\mathbf{P}^{(\omega)}$ (the directional derivative of $\mathbf{P}^{(\omega)}$ with respect to u) is given by the solution of the linearized adjoint equation

$$\begin{cases} -\frac{d}{dt}\delta\mathbf{P}^{(\omega)}(t) = B_u^\omega(t)\delta\mathbf{P}^{(\omega)}(t) + B_\varphi^0(t)\mathbf{P}^{(\omega)}(t), & t \in [0, T], \\ \delta\mathbf{P}^{(\omega)}(T) = \delta\mathbf{M}_\varphi^{(\omega)}(T). \end{cases}$$

This characterization can be derived using formal Lagrangian calculus and rigorously justified using the implicit function theorem; see, e.g., [32, Chapter 1.6].

Since the forward operator S is nonlinear, the problem (2.10) is nonconvex. Hence, convergence of the semismooth Newton method (6.2) to a minimizer u_γ requires a second-order sufficient (local quadratic growth) condition at u_γ for $\gamma > 0$ small, which is difficult to verify. Furthermore, we need to deal with the fact that Newton methods converge only locally, with the convergence region shrinking with γ. For this reason, we perform a continuation in γ, i.e., we solve (2.7) for a sequence $\gamma_1 > \gamma_2 > \cdots$ of regularization parameters, each time using the result for γ_n as initialization for the iteration with γ_{n+1}. In addition, we include in each step of the semismooth Newton method a line search for δu based on the residual norm of the reduced optimality condition (6.1). While globalization of nonsmooth Newton methods is a delicate issue that we do not want to address in this work, we remark that this heuristic approach seems to work well for this problem in practice.

We finally address the discretization of (6.2). The Bloch equation is discretized using a Crank–Nicolson method, where the states $\mathbf{M}^{(\omega)}$ are discretized as continuous piecewise linear functions with values $\mathbf{M}^{(\omega)}_m := \mathbf{M}^{(\omega)}(t_m)$ for discrete time points $t_1, \dots, t_{N_u}$, and the control u is treated as a piecewise constant function, i.e., $u = \sum_{m=1}^{N_u} u_m \chi_{(t_{m-1},t_m]}(t)$, where $\chi_{(a,b]}$ is the characteristic function of the half-open interval $(a, b]$. To obtain a consistent scheme, where discretization and optimization commute, the adjoint state $\mathbf{P}^{(\omega)}$ in (6.3) is discretized as piecewise constant using an appropriate time-stepping scheme [5], and the linearized state $\delta\mathbf{M}^{(\omega)}$ and the linearized adjoint state $\delta\mathbf{P}^{(\omega)}$ are discretized in the same way as the state and adjoint state, respectively; see [1].

6.2 linearized elasticity

For the case of linearized elasticity, we can proceed exactly as in [15, 17]. First, note that due to the embedding $H^1_\Gamma(\Omega) \hookrightarrow L^p(\Omega; \mathbb{R}^2)$ for $p > 2$, the superposition operator H_γ (for $h_\gamma := (\partial g^*)_\gamma$ now given by (4.12)) is again semismooth with Newton derivative $D_N H_\gamma$ (for $D_N h_\gamma$ now given by (4.13)).

To obtain a symmetric Newton system, we reduce (2.7) to the state $y_\gamma = S(u_\gamma)$ and the dual variable p_γ. Since S is a bounded linear operator, we have $S'(u) = S$ and therefore by the definition of S obtain

$$\begin{cases} A^* p_\gamma = z - y_\gamma, \\ A y_\gamma = H_\gamma(p_\gamma), \end{cases}$$

where A denotes the elliptic linear differential operator arising from the system (5.2) of linearized elasticity. Consequently, we consider

$$F(y, p) := \begin{pmatrix} y - z + A^* p \\ Ay - H_\gamma(p) \end{pmatrix} = \begin{pmatrix} 0 \\ 0 \end{pmatrix}, \tag{6.4}$$

where $F : Y \times U^* \to Y \times U$. Since the regularized optimal state y_γ and the adjoint state p_γ are in $H^1_\Gamma(\Omega)$, we may consider $F : H^1_\Gamma(\Omega) \times H^1_\Gamma(\Omega) \to H^1_\Gamma(\Omega)^* \times H^1_\Gamma(\Omega)^*$. For a semismooth Newton step, we obtain $(\delta y, \delta p)$ by solving

$$\begin{pmatrix} \mathrm{Id} & A^* \\ A & -D_N H_\gamma(p^k) \end{pmatrix} \begin{pmatrix} \delta y \\ \delta p \end{pmatrix} = \begin{pmatrix} z - y^k - A^* p^k \\ -Ay^k + H_\gamma(p^k) \end{pmatrix} \tag{6.5}$$

for given (y^k, p^k), and we set $y^{k+1} = y^k + \delta y$ and $p^{k+1} = p^k + \delta p$.

Due to the linearity of the state equation (and hence convexity of the problem), the convergence of the semismooth Newton method for every $\gamma > 0$ to a minimizer of (2.10) can be shown exactly as in [15, 17]. As in the case of the Bloch equation, we include a continuation in γ as well as a line search based on the residual norm in (6.4).

For the discretization, we consider (6.4) in its weak form

$$\begin{pmatrix} \int_\Omega 2\mu\epsilon(p) : \epsilon(\varphi) + \lambda \operatorname{div}(p) \operatorname{div}\varphi + (y-z)\varphi \,\mathrm{d}x \\ \int_\Omega 2\mu\epsilon(y) : \epsilon(\psi) + \lambda \operatorname{div} y \operatorname{div}\psi - h_\gamma(p)\psi \,\mathrm{d}x \end{pmatrix} = \begin{pmatrix} 0 \\ 0 \end{pmatrix} \tag{6.6}$$

for all $\varphi, \psi \in H^1_\Gamma(\Omega)$. We now discretize the state y, the adjoint state p, and the test functions φ_h, ψ_h using piecewise linear finite element functions $y_h, p_h, \varphi_h, \psi_h \in V_h$, where $V_h \subset H^1_\Gamma(\Omega)$ denotes the space of piecewise linear, $\mathbb{R}^2$-valued functions on a uniform triangulation of Ω. Analogously to [15, 17], we employ exact quadrature for all terms except for $\int_\Omega h_\gamma(p_h)\psi_h \,\mathrm{d}x$, which we approximate by $\int_\Omega I_h(h_\gamma(p_h))\psi_h \,\mathrm{d}x$ for the piecewise linear nodal interpolation operator I_h. Thus, letting $\varphi_1, \dots, \varphi_{N_h}$ denote a nodal basis of V_h and introducing the mass and stiffness matrices

$$M_h = \left(\int_\Omega \varphi_i \cdot \varphi_j \,\mathrm{d}x\right)_{ij}, \qquad L_h = \left(\int_\Omega \epsilon(\varphi_i) : \epsilon(\varphi_j) \,\mathrm{d}x\right)_{ij}, \qquad K_h = \left(\int_\Omega \operatorname{div}\varphi_i \cdot \operatorname{div}\varphi_j \,\mathrm{d}x\right)_{ij},$$

as well as $A_h = 2\mu L_h + \lambda K_h$ and the vector $Z_h = (\int_\Omega z \cdot \varphi_1 \,\mathrm{d}x, \dots, \int_\Omega z \cdot \varphi_{N_h} \,\mathrm{d}x)^T$, the discrete version of (6.6) reads

$$\begin{pmatrix} A_h^T \mathbf{p} + M_h \mathbf{y} - Z_h \\ A_h \mathbf{y} - M_h h_\gamma(\mathbf{p}) \end{pmatrix} = \begin{pmatrix} 0 \\ 0 \end{pmatrix},$$

and (6.5) becomes

$$\begin{pmatrix} M_h & A_h^T \\ A_h & -M_h D_N h_\gamma(\mathbf{p}^k) \end{pmatrix} \begin{pmatrix} \delta\mathbf{y} \\ \delta\mathbf{p} \end{pmatrix} = \begin{pmatrix} Z_h - \mathbf{y}^k - A_h^T \mathbf{p}^k \\ -A_h \mathbf{y}^k + M_h h_\gamma(\mathbf{p}^k) \end{pmatrix},$$

where $\mathbf{y} = (y_i)_i$ and $\mathbf{p} = (p_i)_i$ are the nodal values of y_h and p_h, and where $h_\gamma(\mathbf{p}) = (h_\gamma(p_i))_i$ and $D_N h_\gamma(\mathbf{p}) = (D_N h_\gamma(p_i)\delta_{ij})_{ij}$.

6.3 multimaterial branched transport

Here we again follow the same approach as for the Bloch equation, that is, we solve the equation

$$0 = u_\gamma - H_\gamma(-\mathcal{F}'(u_\gamma)) = u_\gamma - H_\gamma(S^*(z - Su_\gamma)).$$

Since u_γ and $S^*(z - Su_\gamma)$ are finite-dimensional, the equation is Newton-differentiable with Newton step $u^{k+1} = u^k + \delta u$ for δu the solution of

$$\left(\operatorname{Id} + D_N H_\gamma(S^*(z - Su^k))S^*S\right)\delta u = -u^k + H_\gamma(S^*(z - Su^k)).$$

Due to the discrete nature of the domain, this is a more challenging problem than for the Bloch equation and therefore requires a more involved path-following. Specifically, during the outer iteration we adapt the reduction factor for γ to keep convergence of the semismooth Newton method within a small number of steps, increasing it if the method requires too many steps (or does not converge at all) and reducing it if the method converges very quickly. In addition, we again employ a line search in δu.

7 numerical examples

We illustrate the proposed approach for the two model problems described in Section 5 and the two specific multibang penalties described in Section 4. The MATLAB code used to generate these examples is available online [20].

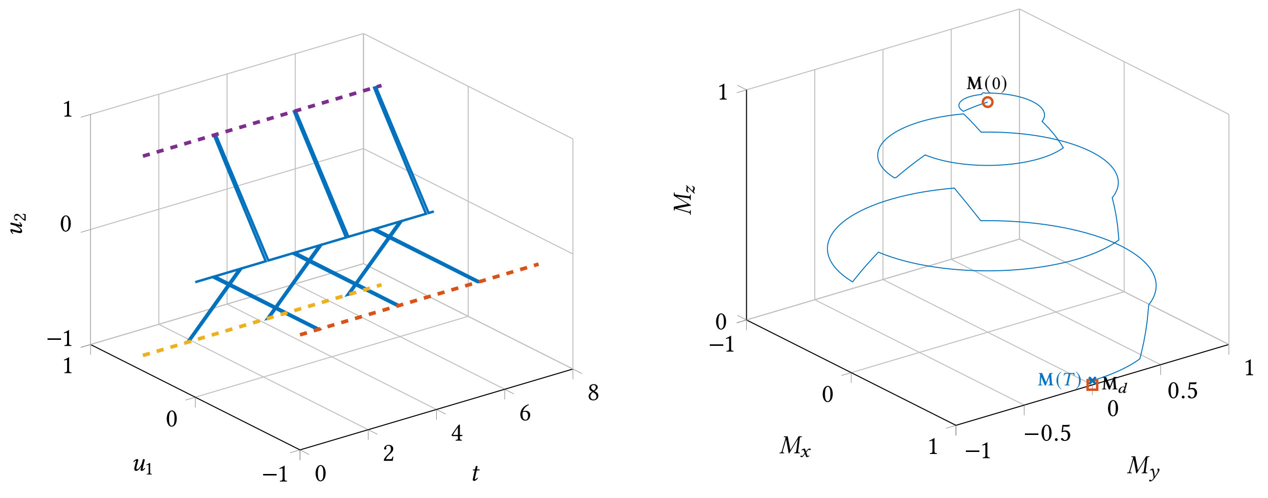

(a) control $\tilde{u}(t)$ (b) state $\mathbf{M}_u^{(\omega)}(t)$

Figure 4: Control and state for the Bloch model problem: $M = 3$

7.1 BLOCH EQUATION

The first example is based on the optimal excitation of isochromats in nuclear magnetic resonance imaging [25], where the aim is to shift the magnetization vector $\mathbf{M}$ at time T from initial alignment with a strong external magnetic field, i.e., $\mathbf{M}(0) = (0, 0, 1)^T$, to the saturated state $\mathbf{M}_d = (1, 0, 0)^T$ using a radiofrequency pulse $u(t) = (\omega_x(t), \omega_y(t))^T$. To follow the physical setup, we scale the controls as $u(t) = \bar{\gamma} B_1 \tilde{u}(t)$, where $\bar{\gamma} \approx 267.51$ is the gyromagnetic ratio (in MHz per Tesla) and $B_1 = 10^{-2}$ is the strength of the modulated magnetic field (in milliTesla); the figures always show the unscaled control $\tilde{u}$. The control cost parameter (which in this setting can be interpreted as a penalty on the specific absorption rate of the radio energy) is set to $\alpha = 10^{-1}$. In all examples, the Bloch equation is discretized with $N_u = 1000$ time intervals; the implementation of the discrete (linearized) Bloch and adjoint equations is taken from [2]. The semismooth Newton iteration is then applied and terminated if the relative or absolute norm of the residual in the optimality condition drops below 10^{-7} or if 500 iterations are exceeded. The Newton step is solved via GMRES without restarts and without preconditioning, which is terminated if the relative residual drops below 10^{-10} or if 1000 iterations are exceeded. The continuation in the Moreau–Yosida regularization is started with $\gamma_0 = 10^2$ and reduced by a factor of $1/2$ until $\gamma_{\min} = 10^{-10}$ is reached or the semismooth Newton iteration fails to converge. We remark that in a practical implementation, these strict fixed tolerances should be replaced as in inexact Newton methods by adaptive criteria based on residuals in the outer loops.

We begin with a single isochromat with $\omega = 10^{-2}\bar{\gamma}$. Figure 4 shows the resulting optimal control $\tilde{u}$ and magnetization evolution $\mathbf{M}^{(\omega)}(t)$ for $M = 3$ equally spaced radially distributed desired control values with magnitude $\omega_0 = 1$ and phases $\theta_1 = -\pi$, $\theta_2 = -\pi/3$, $\theta_3 = \pi/3$, which are marked by colored dashed lines. At any time $t \in [0, T]$, the optimal control $\tilde{u}(t) = (\omega_x(t), \omega_y(t))$ can be seen to only take values from $\mathcal{M}$ as desired. (For easier visual comprehension, $\tilde{u}(t)$ is plotted as a continuous curve so that a jump from one value in $\mathcal{M}$ to another is shown as a connecting line.) Indeed, most of the time we have $\tilde{u} = \bar{u}_0 = 0$, periodically intermitted by short time intervals where $\tilde{u}$ takes the values $\bar{u}_1, \bar{u}_2, \bar{u}_3 \in \mathcal{M}$ in a periodically rotating order. Each of these time intervals coincides in the state trajectory with a change in M_z, while the M_z component of $\mathbf{M}^{(\omega)}$ stays constant during $\tilde{u} = 0$. The final magnetization $\mathbf{M}^{(\omega)}(T)$ shows a very close attainment of the target $\mathbf{M}_d$. The situation is very similar for $M = 6$ with $\omega_0 = 1$ and $\theta \in \{-\pi, -2\pi/3, -\pi/3, 0, \pi/3, 2\pi/3\}$; see Figure 5. In both cases, all nonzero desired control values are made use of equally.

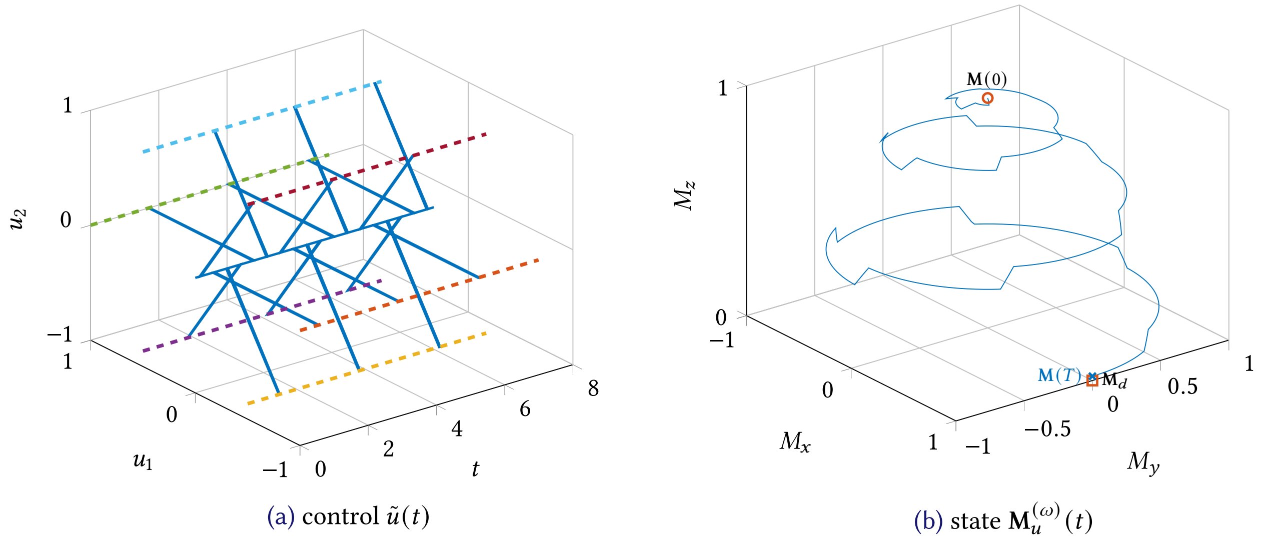

Figure 5: Control and state for the Bloch model problem: $M = 6$

Table 2 summarizes the convergence behavior for the case $M = 3$. For a representative selection of values of γ, it shows the number of semismooth Newton iterations, the average number of GMRES iterations needed to solve a Newton step, the number of times a step of length less than 1 was taken, and the number of nodes t_m for which $u_\gamma(t_m) \notin \mathcal{M}$. For moderate values of γ (approximately $\gamma > 10^{-6}$ in this case), very few iterations of both the semismooth Newton method and the inner GMRES method are required to reach the solution. If γ is decreased further, however, the problem starts becoming significantly more difficult, requiring an increasing number of Newton iterations that, in addition, require a damping to lead to a decrease of the residual. These damped steps typically are taken after a few initial full steps and continue until the region of superlinear convergence is reached, after which the iteration terminates after a small number of full steps. The average number of GMRES steps, however, remains small. For $\gamma < 9.313 \cdot 10^{-8}$, the maximal number of semismooth Newton iterations is no longer sufficient to reach the given tolerance. However, the final row of the table demonstrates that already for $\gamma \approx 10^{-5}$ (where the convergence is still fast), the control is already almost perfectly multibang.

We now consider the simultaneous control of $J = 4$ isochromats with $\omega = 10^{-2}\bar{\gamma} \cdot (1, 2, 3, 4)$. Figure 6 shows the result if the same target $\mathbf{M}_d = (1, 0, 0)^T$ is specified for all isochromats. Again, we have a very close attainment of the target, and again the control is zero most of the time, intermitted by regularly spaced intervals in which nonzero control values from $\mathcal{M}$ are used. This time, not all nonzero values from $\mathcal{M}$ occur, but just $\bar{u}_2$ and $\bar{u}_3$ (indicated by the red and turquoise dashed lines). In addition there are five time points at which control values outside $\mathcal{M}$ are adopted, visible in the graph as short spikes

Table 2: Convergence behavior for the example in Figure 4: number of semi-smooth Newton steps, average number of GMRES iterations to solve a Newton step, number of times a line search was required, and number of nodes t_m with $u_\gamma(t_m) \notin \mathcal{M}$

γ	$1 \cdot 10^2$	2	$2 \cdot 10^{-1}$	$1 \cdot 10^{-2}$	$2 \cdot 10^{-3}$	$2 \cdot 10^{-4}$	$1 \cdot 10^{-5}$	$2 \cdot 10^{-6}$	$9 \cdot 10^{-8}$
# SSN	3	3	4	5	5	5	4	100	101
avg. # GMRES	3	7	7.5	7.4	7.8	8.2	3.8	3.1	4.3
# line search	0	0	0	0	0	0	0	98	99
# not MB	1000	1000	862	376	191	44	3	3	3

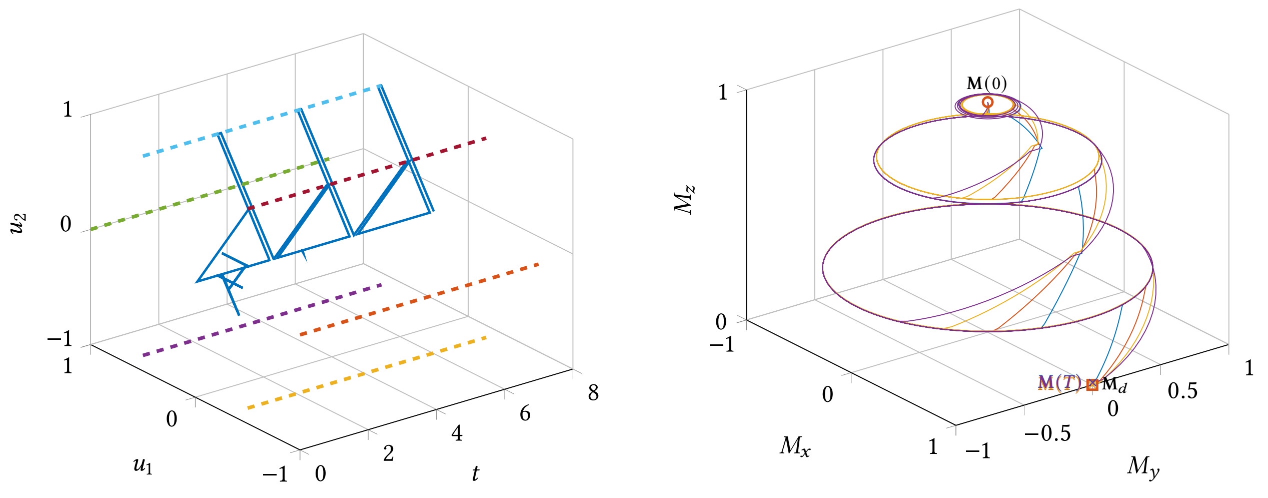

(a) control $\tilde{u}(t)$

(b) state $\mathbf{M}_u^{(\omega_j)}(t)$

Figure 6: Control and state for the Bloch model problem: $M = 6$, $J = 4$

emanating from $\tilde{u} = 0$. (Note, though, that these values still show the desired angles, merely at smaller than desired magnitudes.) This may be due to the fact that in this example, the Newton method has failed to converge already for $\gamma < 2 \cdot 10^{-6}$. In the more realistic case where only a single isochromat – in this case $j = 3$ – is supposed to be excited (i.e., $\mathbf{M}_d = (1, 0, 0)^T$ for $\mathbf{M}^{(\omega_3)}$ and $\mathbf{M}_d = (0, 0, 1)^T$ otherwise), we again obtain a pure multibang control (see Figure 7).

7.2 linearized elasticity

We now address the behavior in the context of optimal control of elliptic partial differential equations for the model equations of two-dimensional linearized elasticity. Here, we choose $\Omega = [0, 1] \times [0, 2]$ and $\Gamma = [0, 1] \times \{0\}$, which models an elastic beam clamped at the bottom. The Lamé parameters are set to $\mu = \frac{E}{2(1+\nu)}$ and $\lambda = \frac{E\nu}{(1+\nu)(1-2\nu)}$ for the elastic modulus $E = 20$ and the Poisson ratio $\nu = 0.3$. We use a uniform structured mesh with 129 vertices in each direction. Since the state equation is linear, we use a direct solver for the Newton step. The Newton iteration is terminated if the active sets (i.e., the case distinctions in the definition of the Moreau–Yosida regularization) for each node coincide for two consecutive iterations, or if 50 iterations are exceeded. The continuation in the regularization parameter γ is performed as for the Bloch equation.

Figure 8 shows the results for six different choices of target, multibang penalty, and control cost parameter. In Figures 8a to 8d, the target displacement $z(x) = R(x - (\frac{1}{2}, 1)^T) - x$ corresponds to a rotation $R \in SO(2)$ of the solid around its center. Figures 8a and 8b use the penalty from Section 4.1 for $\alpha = 10^{-3}$, while Figures 8c and 8d use the penalty from Section 4.2 for $\alpha = 10^{-5}$ and $\alpha = 10^{-3}$, respectively. In all cases, the obtained control makes use of all control values in $\mathcal{M}$ and aligns them with the rotation. Furthermore, the center of the force vortex always lies slightly to the top right of the rotation center of the target state; this allows a stronger overall rightward force in the lower part of the solid to compensate for the clamping at the bottom. Note that unlike the case of (additional) gradient regularization of the control, small patches or sharp corners of the domains with homogeneous force are allowed.

Figure 8e shows that the control is not guaranteed to take values in $\mathcal{M}$; here, the target displacement z is the displacement induced by a deadload to the left applied at the top domain boundary. Since the target was induced by a forcing with zero load throughout the bulk material, the optimal control mainly takes the nonpreferred value of zero. However, a slight random perturbation of z again leads to

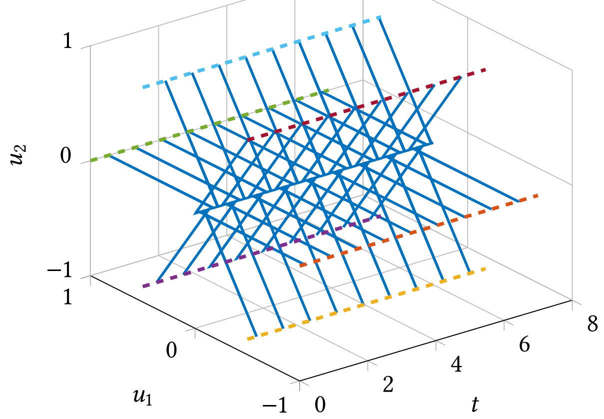

(a) control $\tilde{u}(t)$

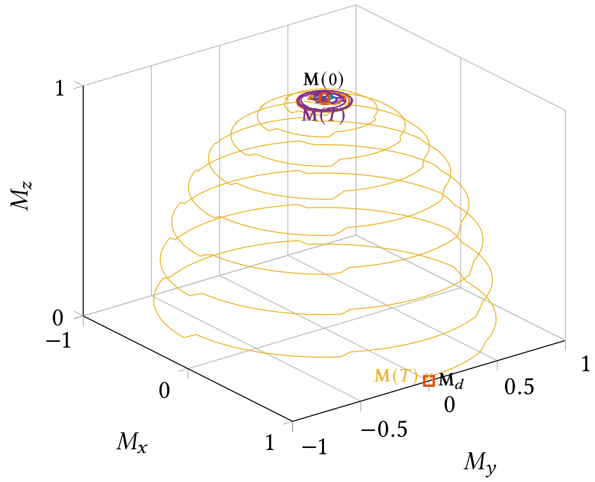

(b) state $\mathbf{M}_u^{(\omega_j)}(t)$

Figure 7: Control and state for the Bloch model problem: $M = 6$, $J = 4$, $\mathbf{M}_d = (0, 0, 1)$ for $j = 3$ and $\mathbf{M}_0$ otherwise

a pure multibang control, as shown in Figure 8f.

We again show the convergence behavior for the example in Figure 8c in Table 3. Since this example is linear, only a few Newton iterations (2 to 6) are required for all values of γ, and correspondingly only a few line searches are carried out for $\gamma < 10^{-5}$. As before, the multibang structure is already strongly promoted for $\gamma \approx 10^{-6}$. (Let us point out that the elastic body is fixed at the bottom boundary so that the control has to be 0 there, which for this example does not lie in $\mathcal{M}$.)

7.3 MULTIMATERIAL BRANCHED TRANSPORT

To illustrate the behavior of our approach for multimaterial branched transport, we fix a random network obtained by a random perturbation of vertices of a regular 10×10 square grid and then performing a Delaunay triangulation (subsequently removing very long edges). In our experiments we fix the vertices that will act as material sources or sinks and assign them different materials, resulting in different optimal transportation schemes; see Figure 9. The amount of each material in our example calculations is simply taken as $m_i = 1$ for all i. In contrast to the previous examples, we here pick $c(v) = |v|_2$ rather than the squared norm, which leads to a preference for combined flows of multiple materials. We fix the control costs at $\alpha = 10^{-3}$.

For the numerical solution, we start with a zero flux and a Moreau–Yosida parameter $\gamma_0 = 20$. The semismooth Newton systems are again solved iteratively using GMRES without restarts at a tolerance of 10^{-11}; we include a backtracking line search with a minimal step size $\tau_{\min} = 10^{-5}$. Starting with a reduction factor $q = 0.5$, we adapt γ and q as follows: If the Newton method for γ_n did not converge

Table 3: Convergence behavior for the example in Figure 8c: number of semi-smooth Newton steps, number of times a line search was required, and number of nodes with $u_\gamma(x) \notin \mathcal{M}$

γ	$2\cdot10^{-1}$	$1\cdot10^{-2}$	$2\cdot10^{-3}$	$2\cdot10^{-4}$	$1\cdot10^{-5}$	$1\cdot10^{-6}$	$2\cdot10^{-7}$	$1\cdot10^{-8}$	$1\cdot10^{-9}$	$2\cdot10^{-10}$
# SSN	2	4	5	5	4	6	4	4	5	6
# line search	0	0	0	0	0	2	1	2	3	4
# not MB	4225	4210	3747	1245	179	84	71	68	68	68

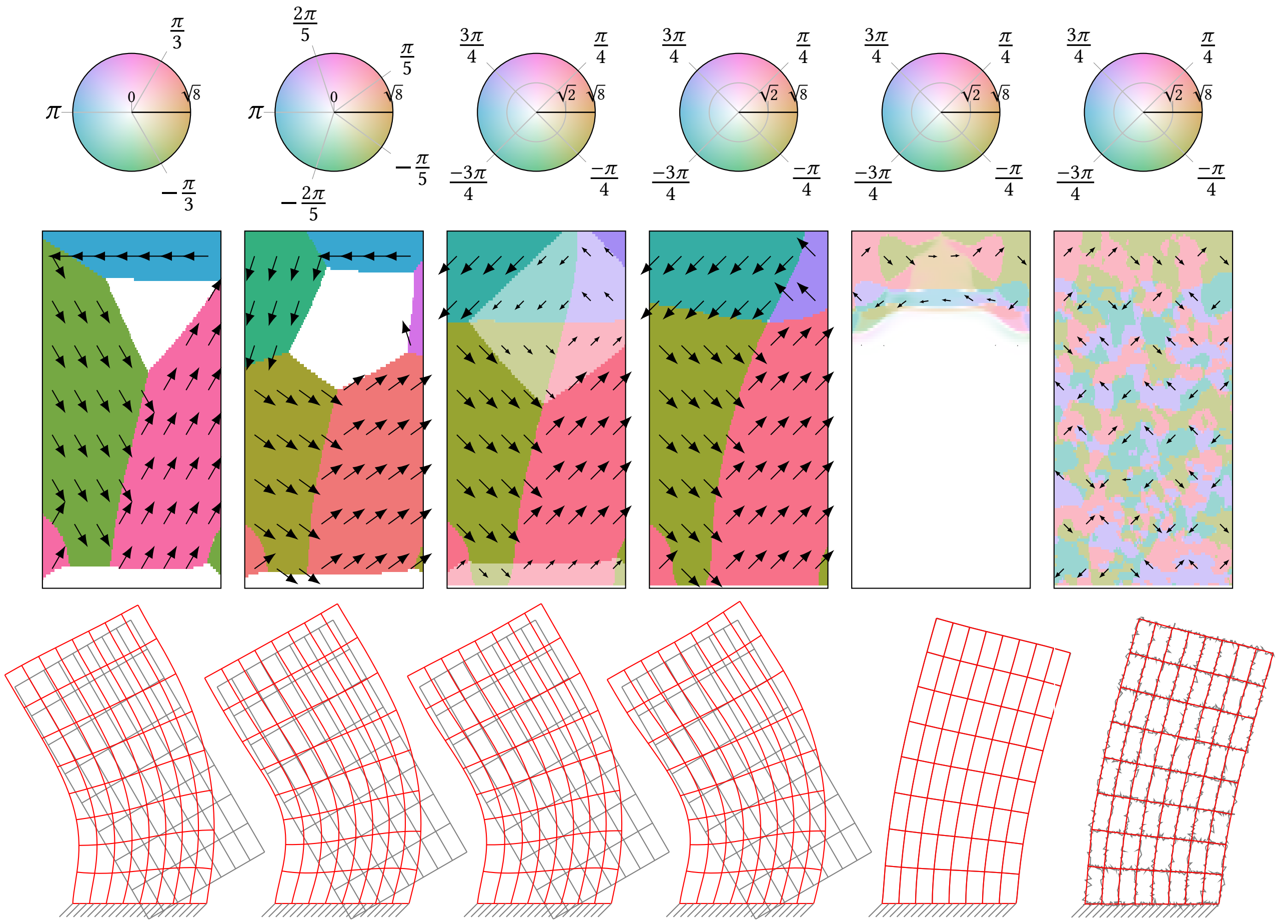

(a) radial, $d = 3$, $\alpha = 10^{-3}$ (b) radial, $d = 5$, $\alpha = 10^{-3}$ (c) concentric, $\alpha = 10^{-3}$ (d) concentric, $\alpha = 10^{-5}$ (e) concentric, $\alpha = 10^{-5}$ (f) concentric, $\alpha = 10^{-5}$

Figure 8: Control (top rows: phase and magnitude color coded as shown in color wheel with values in $\mathcal{M}$ indicated, additionally indicated by arrows) and state (bottom row: target deformation in gray, achieved deformation in red) for the elasticity model problem

within 20 iterations or the minimal step size did not lead to a reduction of the residual norm, we discard the iterate, set $q = q^{0.25}$, and restart with u^{n-1} and $\gamma_{n-1}q$. If the Newton iteration converged (with a residual norm smaller than $\min\{\gamma_n, 10^{-6}\}$ or a relative residual norm smaller than 10^{-9}, whichever occurs first) within 15 steps, we accept the iterate, set $q = \min\{q^{0.75}, 1 - 10^{-4}\}$, and compute u^{n+1} with u^n as starting value and $\gamma_{n+1} = \gamma_n q$. If the Newton iteration even converged within 5 steps, we continue similarly but with reduced $q = \min\{1 - 10^{-3}, \max\{q^{1.25}, 0.5\}\}$. Otherwise we continue with $q = \min\{1 - 10^{-3}, q\}$. We terminate the path-following at $\gamma < 10^{-7}$. Again, this is a heuristic procedure that worked well for this example; in all reported cases, the deviations from the desired discrete control values are less than 0.006 on each edge.

The results are shown in Figure 9 for different configurations of sources and sinks. For three sources at the bottom and three sinks in reversed order at the top, all mass flows converge along the optimal transportation path (Figure 9a). If the flow of m_3 is reversed by swapping its source and sink, there is no longer a payoff by joint transport so that m_3 is transported independently of the other materials (Figure 9b). If instead the order of the sinks is reversed it becomes more economic for m_3 to take the direct route than to create a flow with all materials (Figure 9c). Finally, the network with an additional fourth material becomes more complicated (Figure 9d).

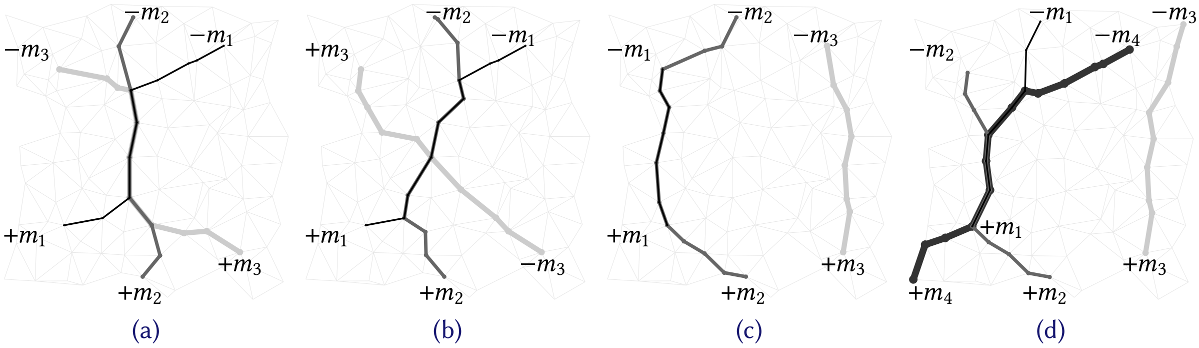

Figure 9: Optimal material flows on a fixed random network with fixed locations but different permutations of sources ($+m_i$) and sinks ($-m_i$); flows corresponding to different materials are indicated by lines of different widths and gray values.

8 CONCLUSION

A preference for a small number of predefined discrete control values can be achieved by a piecewise affine pointwise regularization term whose corners lie at the preferred values. In contrast to the case of scalar controls treated in [17, 18, 16, 19], the case of vector-valued controls allows giving multiple control values equal preference, and numerical experiments for optimal control of the Bloch equation, optimal control of elastic deformation, and multimaterial branched transport show that this feature is indeed exhibited by the optimal control in a broad range of practically relevant scenarios. Furthermore, the optimal control problems leading to admissible controls turn out to be dense among a family of control problems. A more precise characterization of control problems with admissible solutions would be desirable and should be further investigated. For instance, for certain control problems such as the elasticity-based example, one might conjecture that targets leading to nonmultibang controls are nowhere dense. In the context of nonsmooth optimization, investigating rigorous globalization of the semismooth Newton method by the path-following approach followed for the branched transport example would be worthwhile. Finally, an interesting topic for follow-up work would be combining the vector-valued results presented in this work with the techniques from [16] for topology optimization of elastic composite materials.

APPENDIX A PROPERTIES OF THE BLOCH EQUATION

Here we verify that the state operator (5.1) satisfies the required assumptions (A1)–(A4). In the following, a subscript to $\mathbf{M}^{(\omega)}$ and $\mathbf{B}^{(\omega)}$ always refers to the chosen control u.

Proposition A.1. *The operator S as defined in (5.1) is well-defined and satisfies (A1)–(A3).*

Proof. Introducing the skew-symmetric matrix

$$B_u^{\omega}(t) = \begin{pmatrix} 0 & \omega & -(u(t))_2 \\ -\omega & 0 & (u(t))_1 \\ (u(t))_2 & -(u(t))_1 & 0 \end{pmatrix},$$

the homogeneous linear Bloch equation $\frac{\mathrm{d}}{\mathrm{d}t}\mathbf{M}_u^{(\omega)}(t) = B_u^{\omega}(t)\mathbf{M}_u^{(\omega)}(t)$ for a control $u(t) \in \mathbb{R}^2$ has a solution $\mathbf{M}_u^{(\omega)}(t)$ by Carathéodory's existence theorem. Furthermore,

$$\frac{\mathrm{d}}{\mathrm{d}t}|\mathbf{M}_u^{(\omega)}(t)|_2^2 = 2\mathbf{M}_u^{(\omega)}(t) \cdot \frac{\mathrm{d}}{\mathrm{d}t}\mathbf{M}_u^{(\omega)}(t) = 0,$$

and thus $|\mathbf{M}_u^{(\omega)}(t)|_2 = 1$ for all t. Now let $u_i \rightharpoonup u$ weakly in $L^2(\Omega;\mathbb{R}^2)$. Then

$$\begin{cases} \dfrac{\mathrm{d}}{\mathrm{d}t}\mathbf{M}_{u_i}^{(\omega)}(t) - \dfrac{\mathrm{d}}{\mathrm{d}t}\mathbf{M}_u^{(\omega)}(t) = B_{u_i}^{\omega}(t)\left(\mathbf{M}_{u_i}^{(\omega)}(t) - \mathbf{M}_u^{(\omega)}(t)\right) + (B_{u_i}^{\omega}(t) - B_u^{\omega}(t))\mathbf{M}_u^{(\omega)}(t), \quad t \in [0,T], \\ \qquad\qquad \mathbf{M}_{u_i}^{(\omega)}(0) = \mathbf{M}_u^{(\omega)}(0). \end{cases}$$

Upon abbreviating $\Delta M_i = \mathbf{M}_{u_i}^{(\omega)} - \mathbf{M}_u^{(\omega)}$ and $\Delta B_i = (B_{u_i}^{\omega} - B_u^{\omega})\mathbf{M}_u^{(\omega)}$ and integrating from 0 to t, we arrive at

$$\begin{aligned} |\Delta M_i(t)|_2 &= \left| \int_0^t B_{u_i}^{\omega}(s)\Delta M_i(s)\,\mathrm{d}s + \int_0^t \Delta B_i(s)\,\mathrm{d}s \right|_2 \\ &\leq \int_0^t |B_{u_i}^{\omega}(s)|_2 |\Delta M_i(s)|_2\,\mathrm{d}s + \left| \int_0^t \Delta B_i(s)\,\mathrm{d}s \right|_2 . \end{aligned}$$

Gronwall's inequality now implies that

$$\text{(A.1)} \qquad |\Delta M_i(t)|_2 \leq \left| \int_0^t \Delta B_i(s)\,\mathrm{d}s \right|_2 + \int_0^t \left| \int_0^r \Delta B_i(s)\,\mathrm{d}s \right|_2 |B_{u_i}^{\omega}(r)|_2 \exp\left(\int_r^t |B_{u_i}^{\omega}(s)|_2\,\mathrm{d}s \right) \mathrm{d}r.$$

The first term converges to zero due to $\Delta B_i \rightharpoonup 0$ in $L^2(\Omega;\mathbb{R}^3)$ (since $\mathbf{M}_u^{(\omega)} \in L^\infty(\Omega;\mathbb{R}^3)$). Additionally, the exponential is bounded by $\exp(\sqrt{T}\|B_{u_i}^{\omega}\|_{L^2(\Omega;\mathbb{R}^{3\times3})}) \leq C \in \mathbb{R}$ independent of i. Thus, the right-hand side converges to zero if

$$f_i \to 0 \text{ in } L^2(\Omega;\mathbb{R}) \qquad \text{for} \qquad f_i : \Omega \to \mathbb{R}, \quad r \mapsto \int_0^r \Delta B_i(s)\,\mathrm{d}s.$$

This is indeed the case since

$$\|f_i\|_{L^2(\Omega)}^2 = \int_{\{s\in(0,T)^3 : s_1,s_2\leq s_3\}} \Delta B_i(s_1)\cdot\Delta B_i(s_2)\,\mathrm{d}s$$

and $s \mapsto \Delta B_i(s_1)\cdot\Delta B_i(s_2)$ converges weakly to zero in $L^2((0,T)^3;\mathbb{R})$. Thus $\mathbf{M}_{u_i}^{(\omega_j)}(T)$ converges for all j, and therefore $S(u_i) \to S(u)$. This argument also implies uniqueness of the solution.

Moreover, S is Fréchet differentiable, and its derivative at $u \in L^2(\Omega;\mathbb{R}^2)$ is given by

$$S'(u) : U \to Y, \quad \varphi \mapsto \delta\mathbf{M}_\varphi(T) = (\delta\mathbf{M}_\varphi^{(\omega_1)}(T), \ldots, \delta\mathbf{M}_\varphi^{(\omega_J)}(T))$$

with $\delta\mathbf{M}_\varphi^{(\omega)}$ solving the linearized state equation (note $\partial_u(B_u^{\omega})(\varphi) = B_\varphi^0$)

$$\text{(A.2)} \qquad \begin{cases} \frac{\mathrm{d}}{\mathrm{d}t}\delta\mathbf{M}_\varphi^{(\omega)}(t) = B_u^{\omega}(t)\delta\mathbf{M}_\varphi^{(\omega)}(t) + B_\varphi^0(t)\mathbf{M}_u^{(\omega)}(t), \qquad t \in [0,T], \\ \delta\mathbf{M}_\varphi^{(\omega)}(0) = (0,0,0)^T. \end{cases}$$

Indeed, $\delta\mathbf{M}_\varphi(T)$ is obviously linear in φ, and the unique solvability follows just like for $\mathbf{M}_u^{(\omega)}$. Furthermore, for any $\tilde{u} \in U$ with $\|\tilde{u} - u\|_U \leq 1$ and $\varphi = \tilde{u} - u$ we have

$$\tfrac{\mathrm{d}}{\mathrm{d}t}(\mathbf{M}_{\tilde{u}}^{(\omega)} - \mathbf{M}_u^{(\omega)} - \delta\mathbf{M}_\varphi^{(\omega)}) = B_{\tilde{u}}^{\omega}(\mathbf{M}_{\tilde{u}}^{(\omega)} - \mathbf{M}_u^{(\omega)} - \delta\mathbf{M}_\varphi^{(\omega)}) + (B_{\tilde{u}}^{\omega} - B_u^{\omega})\delta\mathbf{M}_\varphi^{(\omega)}$$

with zero initial condition. Gronwall estimates analogous to (A.1) (now for $\delta\mathbf{M}_\varphi^{(\omega)}$ and $\mathbf{M}_{\tilde{u}}^{(\omega)} - \mathbf{M}_u^{(\omega)} - \delta\mathbf{M}_\varphi^{(\omega)}$, exploiting that $|B_{\tilde{u}}^{\omega}(r)|_2 \exp(\int_r^t |B_{\tilde{u}}^{\omega}(s)|_2\,\mathrm{d}s)$ is bounded by a constant only depending on $\|u\|_U$) imply that

$$|\delta\mathbf{M}_\varphi^{(\omega)}(t)|_2 \leq \tilde{C}\|B_{\tilde{u}}^{\omega} - B_u^{\omega}\|_{L^2(\Omega;\mathbb{R}^{3\times3})} \leq 2\tilde{C}\|\tilde{u} - u\|_U$$

for a constant $\tilde{C} > 0$ and all $t \in \Omega$ as well as

$$\begin{aligned}|\mathbf{M}_{\tilde{u}}^{(\omega)}(T) - \mathbf{M}_{u}^{(\omega)}(T) - \delta\mathbf{M}_{\varphi}^{(\omega)}(T)|_2 &\leq C \sup_{t\in\Omega}\left|\int_0^t (B_{\tilde{u}}^{\omega}(s) - B_u^{\omega}(s))\delta\mathbf{M}_{\varphi}^{(\omega)}(s)\,\mathrm{d}s\right|_2 \\ &\leq C\|B_{\tilde{u}}^{\omega} - B_u^{\omega}\|_{L^1(\Omega;\mathbb{R}^{3\times3})}\|\delta\mathbf{M}_{\varphi}^{(\omega)}\|_{L^\infty(\Omega;\mathbb{R}^3)} \\ &\leq C\|\tilde{u} - u\|_U^2,\end{aligned}$$

where C denotes a positive constant (not necessarily the same in all inequalities). We thus have

$$|S(\tilde{u}) - S(u) - S'(u)(\tilde{u} - u)|_2 \leq C\|\tilde{u} - u\|_U^2$$

as required. The compactness follows from the finite dimensionality of $\operatorname{ran} S$. □

We will also require some regularity results for the adjoint operator $S'(u)^*$.

Proposition A.2. *For S from (5.1) and $u \in U$ we have*

$$\begin{aligned}&S'(u)^* : Y \to U,\\ &(S'(u)^*y)(t) = \sum_{j=1}^J \begin{pmatrix} 0 & \left(\mathbf{M}_u^{(\omega_j)}(t)\right)_3 & -\left(\mathbf{M}_u^{(\omega_j)}(t)\right)_2 \\ -\left(\mathbf{M}_u^{(\omega_j)}(t)\right)_3 & 0 & \left(\mathbf{M}_u^{(\omega_j)}(t)\right)_1\end{pmatrix}\mathbf{\Psi}_{u,j}(t),\end{aligned}$$

where $\mathbf{\Psi}_{u,j}$ solves the adjoint equation

$$\frac{\mathrm{d}}{\mathrm{d}t}\mathbf{\Psi}_{u,j}(t) = \mathbf{\Psi}_{u,j}(t) \times \mathbf{B}_u^{(\omega_j)}(t), \quad \mathbf{\Psi}_{u,j}(T) = y_j, \quad j = 1, \ldots, J.$$

Proof. From Proposition A.1 we have $S'(u)\varphi = (\delta\mathbf{M}_{\varphi}^{(\omega_1)}(T), \ldots, \delta\mathbf{M}_{\varphi}^{(\omega_J)}(T))$ for any $u, \varphi \in U$ with $\delta\mathbf{M}_{\varphi}^{(\omega)}$ solving (A.2). Thus we obtain for $y \in (\mathbb{R}^3)^J$ that

$$\begin{aligned}\int_\Omega \varphi(t)\cdot(S'(u)^*y)(t)\,\mathrm{d}t = \langle y, S'(u)\varphi\rangle &= \sum_{j=1}^J y_j^T\delta\mathbf{M}_{\varphi}^{(\omega_j)}(T)\\ &= \sum_{j=1}^J \mathbf{\Psi}_{u,j}(T)^T\delta\mathbf{M}_{\varphi}^{(\omega_j)}(T)\\ &= \sum_{j=1}^J\int_\Omega \mathbf{\Psi}_{u,j}(t)^T\frac{\mathrm{d}}{\mathrm{d}t}\delta\mathbf{M}_{\varphi}^{(\omega_j)}(t) + \frac{\mathrm{d}}{\mathrm{d}t}\mathbf{\Psi}_{u,j}(t)^T\delta\mathbf{M}_{\varphi}^{(\omega_j)}(t)\,\mathrm{d}t\\ &= \sum_{j=1}^J\int_\Omega \mathbf{\Psi}_{u,j}(t)^T\left[\frac{\mathrm{d}}{\mathrm{d}t}\delta\mathbf{M}_{\varphi}^{(\omega_j)}(t) - \delta\mathbf{M}_{\varphi}^{(\omega_j)}(t)\times\mathbf{B}_u^{\omega_j}(t)\right]\mathrm{d}t\\ &= \sum_{j=1}^J\int_\Omega \mathbf{\Psi}_{u,j}(t)^T\left[B_{\varphi}^0(t)\mathbf{M}_u^{(\omega_j)}(t)\right]\mathrm{d}t\end{aligned}$$

from which the result follows. □

Proposition A.3. *For any $u \in U$, we have $\operatorname{ran} S'(u)^* \hookrightarrow L^\infty(\Omega;\mathbb{R}^2)$. Moreover, $u \mapsto S'(u)^*$ is continuous in $L^\infty(\Omega;\mathbb{R}^2)$ under weak convergence of u in U and thus it satisfies (A4) with $V = L^1(\Omega;\mathbb{R}^2)$.*

Proof. By the formula for $S'(u)^*$ from Proposition A.2, it is enough to show that $\mathbf{M}_{u_i}^{(\omega_j)}$ and $\mathbf{\Psi}_{u_i,j}$ converge in $L^\infty(\Omega;\mathbb{R}^3)$ as $u_i \rightharpoonup u$ in U. It suffices to consider $\mathbf{M}_{u_i}^{(\omega_j)}$, since the adjoint variable $\mathbf{\Psi}_{u,j}$ satisfies the same differential equation. Thus, we only have to show that the right-hand side in (A.1) converges to zero uniformly in t. Note that the second integral is bounded above by the one for $t = T$ which has already been shown to converge to zero. Hence it suffices to show $\int_0^t \Delta B_i(s)\,\mathrm{d}s \to 0$ uniformly in t as $i \to \infty$. Since $\Delta B_i \rightharpoonup 0$ in $L^2(\Omega;\mathbb{R}^3)$, we also have weak convergence in $L^1(\Omega;\mathbb{R}^3)$ so that by the Dunford–Pettis criterion the ΔB_i are equi-integrable. Now let $t_i \in [0,T]$ be such that $|\int_0^{t_i} \Delta B_i(s)\,\mathrm{d}s|_2 \geq \sup_{t\in[0,T]} |\int_0^t \Delta B_i(s)\,\mathrm{d}s|_2 - \frac{1}{i}$, and assume that for a subsequence (still indexed by i) we have $|\int_0^{t_i} \Delta B_i(s)\,\mathrm{d}s|_2 \geq C > 0$ for all i. Upon taking another subsequence, we can further assume that $t_i \to \hat{t} \in [0,T]$. Due to the equi-integrability, there is a $\Delta t > 0$ such that $\int_{\hat{t}-\Delta t}^{\hat{t}+\Delta t} |\Delta B_i(s)|_2\,\mathrm{d}s < C/2$; thus for i large enough we have $|\int_0^{\hat{t}} \Delta B_i(s)\,\mathrm{d}s|_2 \geq C/2$. However, this contradicts the weak convergence of ΔB_i to 0 so that indeed $\int_0^t \Delta B_i(s)\,\mathrm{d}s \to 0$ uniformly in t as $i \to \infty$. □

REFERENCES

[1] C. Aigner, C. Clason, A. Rund, and R. Stollberger, Efficient high-resolution RF pulse design applied to simultaneous multi-slice excitation, *Journal of Magnetic Resonance* 263 (2016), 33–44, doi:10.1016/j.jmr.2015.11.013.

[2] C. S. Aigner, C. Clason, and A. Rund, rfcontrol, Online resource on Zenodo, 2015, doi:10.5281/zenodo.31187.

[3] C. K. Anand, A. D. Bain, A. T. Curtis, and Z. Nie, Designing optimal universal pulses using second-order, large-scale, non-linear optimization, *Journal of Magnetic Resonance* 219 (2012), 61–74, doi:10.1016/j.jmr.2012.04.004.

[4] H. H. Bauschke and P. L. Combettes, *Convex Analysis and Monotone Operator Theory in Hilbert Spaces*, Springer, New York, 2011, doi:10.1007/978-1-4419-9467-7.

[5] R. Becker, D. Meidner, and B. Vexler, Efficient numerical solution of parabolic optimization problems by finite element methods, *Optimization Methods and Software* 22 (2007), 813–833, doi:10.1080/10556780701228532.

[6] M. Bergounioux and F. Tröltzsch, Optimality conditions and generalized bang-bang principle for a state-constrained semilinear parabolic problem, *Numerical Functional Analysis and Optimization* 17 (1996), 517–536, doi:10.1080/01630569608816708.

[7] M. Bernot, V. Caselles, and J. M. Morel, *Optimal Transportation Networks*, volume 1955 of Lecture Notes in Mathematics, Springer-Verlag, Berlin, 2009, doi:10.1007/978-3-540-69315-4.

[8] B. Bonnard, M. Claeys, O. Cots, and P. Martinon, Geometric and nUmerical methods in the contrast imaging problem in nuclear magnetic resonance, *Acta Applicandae Mathematicae* 135 (2014), 5–45, doi:10.1007/s10440-014-9947-3.

[9] D. Braess, *Finite Elements*, Cambridge University Press, Cambridge, third edition, 2007, doi:10.1017/cbo9780511618635.

[10] A. Braides, *Γ-Convergence for Beginners*, volume 22 of Oxford Lecture Series in Mathematics and its Applications, Oxford University Press, Oxford, 2002.

[11] E. Casas, R. Herzog, and G. Wachsmuth, Optimality conditions and error analysis of semilinear elliptic control problems with L^1 cost functional, *SIAM Journal on Optimization* 22 (2012), 795–820, doi:10.1137/110834366.

[12] F. Clarke, *Functional Analysis, Calculus of Variations and Optimal Control*, Springer, London, 2013, doi:10.1007/978-1-4471-4820-3.

[13] C. Clason and T. B. T. Do, Convex regularization of discrete-valued inverse problems, in *New Trends in Parameter Identification for Mathematical Models*, B. Hofmann, A. Leitão, and J. Zubelli (eds.), Trends in Mathematics, Springer, 2018, 31–51, doi:10.1007/978-3-319-70824-9_2.

[14] C. Clason, T. B. T. Do, and F. Pörner, Error estimates for the approximation of multibang control problems, *Computational Optimization and Applications* 71 (2018), 857–878, doi:10.1007/s10589-018-0026-y.

[15] C. Clason, K. Ito, and K. Kunisch, A convex analysis approach to optimal controls with switching structure for partial differential equations, *ESAIM: Control, Optimisation and Calculus of Variations* 22 (2016), 581–609, doi:10.1051/cocv/2015017.

[16] C. Clason, F. Kruse, and K. Kunisch, Total variation regularization of multi-material topology optimization, *ESAIM: Mathematical Modelling and Numerical Analysis* 52 (2018), 275–303, doi:10.1051/m2an/2017061.

[17] C. Clason and K. Kunisch, Multi-bang control of elliptic systems, *Annales de l'Institut Henri Poincaré (C) Analyse Non Linéaire* 31 (2014), 1109–1130, doi:10.1016/j.anihpc.2013.08.005.

[18] C. Clason and K. Kunisch, A convex analysis approach to multi-material topology optimization, *ESAIM: Mathematical Modelling and Numerical Analysis* 50 (2016), 1917–1936, doi:10.1051/m2an/2016012.

[19] C. Clason, K. Kunisch, and P. Trautmann, Optimal control of the principal coefficient in a scalar wave equation, *Applied Mathematics & Optimization* (2020), doi:10.1007/s00245-020-09733-9.

[20] C. Clason, C. Tameling, and B. Wirth, vectormultibang, Online resource on Zenodo, 2021, doi:10.5281/zenodo.4803687.

[21] C. Clason and T. Valkonen, Introduction to Nonsmooth Analysis and Optimization, 2020, arXiv:2020.00216v3.

[22] S. Conolly, D. Nishimura, and A. Macovski, Optimal control solutions to the magnetic resonance selective excitation problem, *IEEE Transactions on Medical Imaging* 5 (1986), 106–115, doi:10.1109/tmi.1986.4307754.

[23] P. A. S. Cruickshank, D. R. Bolton, D. A. Robertson, R. I. Hunter, R. J. Wylde, and G. M. Smith, A kilowatt pulsed 94 GHz electron paramagnetic resonance spectrometer with high concentration sensitivity, high instantaneous bandwidth, and low dead time, *Review of Scientific Instruments* 80 (2009), 103102, doi:10.1063/1.3239402.

[24] T. B. T. Do, *Discrete Regularization for Parameter Identification Problems*, PhD thesis, Faculty of Mathematics, University of Duisburg-Essen, 2019, doi:10.17185/duepublico/70265.

[25] G. Dridi, M. Lapert, J. Salomon, S. J. Glaser, and D. Sugny, Discrete-valued-pulse optimal control algorithms: Application to spin systems, *Physical Review A* 92 (2015), 043417, doi:10.1103/physreva.92.043417.

[26] I. Ekeland and R. Témam, *Convex Analysis and Variational Problems*, volume 28 of Classics Appl. Math., SIAM, Philadelphia, 1999, doi:10.1137/1.9781611971088.

[27] C. Epstein and F. Wehrli, Magnetic Resonance Imaging, in *Encyclopedia of Mathematical Physics*, J. P. Françoise, G. L. Naber, and T. S. Tsun (eds.), Academic Press, Oxford, 2006, 367–375, doi:http://dx.doi.org/10.1016/b0-12-512666-2/00348-5.

[28] K. Fukuda, T. M. Liebling, and F. Margot, Analysis of backtrack algorithms for listing all vertices and all faces of a convex polyhedron, *Computational Geometry* 8 (1997), 1–12, doi:10.1016/0925-7721(95)00049-6.

[29] N. I. Gershenzon, D. F. Miller, and T. E. Skinner, The design of excitation pulses for spin systems using optimal control theory: with application to NMR spectroscopy, *Optimal Control Applications and Methods* 30 (2009), 463–475, doi:10.1002/oca.867.

[30] W. Grissom, Dan Xu, A. Kerr, J. Fessler, and D. Noll, Fast large-tip-angle multidimensional and parallel RF pulse design in MRI, *IEEE Transactions on Medical Imaging* 28 (2009), 1548–1559, doi:10.1109/tmi.2009.2020064.

[31] W. A. Grissom, K. Setsompop, S. A. Hurley, J. Tsao, J. V. Velikina, and A. A. Samsonov, Advancing RF pulse design using an open-competition format: Report from the 2015 ISMRM challenge, *Magnetic Resonance in Medicine* 78 (2017), 1352–1361, doi:10.1002/mrm.26512.

[32] M. Hinze, R. Pinnau, M. Ulbrich, and S. Ulbrich, *Optimization with PDE constraints*, Springer, New York, 2009, doi:10.1007/978-1-4020-8839-1.

[33] S. Holman and P. Richardson, SPECT with a multi-bang assumption on attenuation, *Inverse Problems* 36 (2020), 125005, doi:10.1088/1361-6420/abab59.

[34] K. Ito and K. Kunisch, *Lagrange Multiplier Approach to Variational Problems and Applications*, volume 15 of Advances in Design and Control, SIAM, Philadelphia, 2008, doi:10.1137/1.9780898718614.

[35] K. Ito and K. Kunisch, Optimal control with $L^p(\Omega)$, $p \in [0,1)$ control cost, *SIAM Journal on Control and Optimization* 52 (2014), 1251–1275, doi:10.1137/120896529.

[36] N. Khaneja, T. Reiss, C. Kehlet, T. Schulte-Herbrüggen, and S. J. Glaser, Optimal control of coupled spin dynamics: design of NMR pulse sequences by gradient ascent algorithms, *Journal of Magnetic Resonance* 172 (2005), 296–305, doi:10.1016/j.jmr.2004.11.004.

[37] J. Mao, T. H. Mareci, K. N. Scott, and E. R. Andrew, Selective inversion radiofrequency pulses by optimal control, *Journal of Magnetic Resonance (1969)* 70 (1986), 310–318, doi:10.1016/0022-2364(86)90016-8.

[38] A. Marchese, A. Massaccesi, and R. Tione, A multimaterial transport problem and its convex relaxation via rectifiable G-currents, *SIAM Journal on Mathematical Analysis* 51 (2019), 1965–1998, doi:10.1137/17m1162858.

[39] A. Massaccesi, E. Oudet, and B. Velichkov, Numerical calibration of Steiner trees, *Applied Mathematics & Optimization* 79 (2019), 69–86, doi:10.1007/s00245-017-9421-5.

[40] A. L. Mazzucato and V. Nistor, Well-posedness and regularity for the elasticity equation with mixed boundary conditions on polyhedral domains and domains with cracks, *Arch. Ration. Mech. Anal.* 195 (2010), 25–73, doi:10.1007/s00205-008-0180-y.

[41] S. Nicaise, About the Lamé system in a polygonal or a polyhedral domain and a coupled problem between the Lamé system and the plate equation. I. Regularity of the solutions, *Ann. Scuola Norm. Sup. Pisa Cl. Sci. (4)* 19 (1992), 327–361, http://www.numdam.org/item?id=ASNSP_1992_4_19_3_327_0.

[42] R. Prigl and U. Haeberlen, The theoretical and practical limits of resolution in multiple-pulse high-resolution NMR of solids, in *Advances in Magnetic and Optical Resonance*, W. S. Warren (ed.), volume 19, Academic Press, 1996, 1–58, doi:10.1016/s1057-2732(96)80017-9.

[43] D. Rosenfeld and Y. Zur, Design of adiabatic selective pulses using optimal control theory, *Magnetic Resonance in Medicine* 36 (1996), 401–409, doi:10.1002/mrm.1910360311.

[44] W. Schirotzek, *Nonsmooth Analysis*, Springer, Berlin, 2007, doi:10.1007/978-3-540-71333-3.

[45] T. E. Skinner, N. I. Gershenzon, M. Nimbalkar, W. Bermel, B. Luy, and S. J. Glaser, New strategies for designing robust universal rotation pulses: Application to broadband refocusing at low power, *Journal of Magnetic Resonance* 216 (2012), 78–87, doi:10.1016/j.jmr.2012.01.005.

[46] V. Smith, J. Kurhanewicz, and T. L. James, Solvent-suppression pulses. I. Design using optimal control theory, *Journal of Magnetic Resonance (1969)* 95 (1991), 41–60, doi:10.1016/0022-2364(91)90323-l.

[47] G. Stadler, Elliptic optimal control problems with L^1-control cost and applications for the placement of control devices, *Computational Optimization and Applications* 44 (2007), 159, doi:10.1007/s10589-007-9150-9.

[48] D. Tiba, *Optimal Control of Nonsmooth Distributed Parameter Systems*, volume 1459 of Lecture Notes in Mathematics, Springer, Berlin, Heidelberg, 1990, doi:10.1007/bfb0085564.

[49] F. Tröltzsch, A minimum principle and a generalized bang-bang-principle for a distributed optimal control problem with constraints on control and state, *ZAMM – Journal of Applied Mathematics and Mechanics / Zeitschrift für Angewandte Mathematik und Mechanik* 59 (1979), 737–739, doi:10.1002/zamm.19790591208.

[50] M. Ulbrich, *Semismooth Newton Methods for Variational Inequalities and Constrained Optimization Problems in Function Spaces*, volume 11 of MOS-SIAM Series on Optimization, SIAM, Philadelphia, 2011, doi:10.1137/1.9781611970692.

[51] M. S. Vinding, I. I. Maximov, Z. Tošner, and N. C. Nielsen, Fast numerical design of spatial-selective RF pulses in MRI using Krotov and quasi-Newton based optimal control methods, *The Journal of Chemical Physics* 137 (2012), 054203, doi:10.1063/1.4739755.

[52] J. Webber and E. L. Miller, A novel reconstruction technique for two-dimensional Bragg scatter imaging, in *Anomaly Detection and Imaging with X-Rays (ADIX) VI*, A. Ashok, J. A. Greenberg, and M. E. Gehm (eds.), volume 11738, SPIE, 2021, doi:10.1117/12.2589013.

[53] D. Xu, K. F. King, Y. Zhu, G. C. McKinnon, and Z. P. Liang, Designing multichannel, multidimensional, arbitrary flip angle RF pulses using an optimal control approach, *Magnetic Resonance in Medicine* 59 (2008), 547–560, doi:10.1002/mrm.21485.